Research Square

Preprints are preliminary reports that have not undergone peer review.
They should not be considered conclusive, used to inform clinical practice,
or referenced by the media as validated information.

A vitamin cross-feeding mechanism mediates microbial niche adaptation on leaves

Yiheng Hu

yiheng.hu@zmbp.uni-tuebingen.de

University of Tuebingen https://orcid.org/0000-0002-6513-9834

Johanna Bode

Department of Microbial Interactions, Centre of Plant Molecular Biology (ZMBP), Eberhard-Karls-University of Tübingen, Tübingen, Germany

Daniel Gómez-Pérez

Department of Microbial Interactions, Centre of Plant Molecular Biology (ZMBP), Eberhard-Karls-University of Tübingen, Tübingen, Germany

Marco Guerreiro

Botanical Institute, Christian-Albrechts University of Kiel, Kiel, Germany https://orcid.org/0000-0002-5133-8779

Alfredo Mari

Department of Microbial Interactions, Centre of Plant Molecular Biology (ZMBP), Eberhard-Karls-University of Tübingen, Tübingen, Germany

Kun Wang

Department of Microbial Interactions, Centre of Plant Molecular Biology (ZMBP), Eberhard-Karls-University of Tübingen, Tübingen, Germany

Sinja Niemann

Department of Microbial Interactions, Centre of Plant Molecular Biology (ZMBP), Eberhard-Karls-University of Tübingen, Tübingen, Germany https://orcid.org/0009-0004-1433-2951

Maryam Mahmoudi

Department of Microbial Interactions, Centre of Plant Molecular Biology (ZMBP), Eberhard-Karls-University of Tübingen, Tübingen, Germany

Ariane Kemen

Department of Microbial Interactions, Centre of Plant Molecular Biology (ZMBP), Eberhard-Karls-University of Tübingen, Tübingen, Germany

Paloma Duran

Department of Plant Microbe Interactions, Max Planck Institute for Plant Breeding Research, Cologne, Germany

Oskar Wacker

Quantitative Biology Center (QBiC), University of Tübingen, Tübingen, Germany https://orcid.org/0009-0003-2041-610X

Daniel Straub
Quantitative Biology Center (QBiC), University of Tübingen, Tübingen, Germany

Sven Nahnsen
Quantitative Biology Center (QBiC), The M3 Research Centre https://orcid.org/0000-0002-4375-0691

Benjamin Schwessinger
The Sainsbury Laboratory

Fabrice Roux
CNRS https://orcid.org/0000-0001-8059-5638

Carlos Alonso-Blanco
CNB-CSIC, Madrid https://orcid.org/0000-0002-4738-5556

Jon Ågren
Uppsala University https://orcid.org/0000-0001-9573-2463

Stéphane Hacquard
Max Planck Institute for Plant Breeding Research https://orcid.org/0000-0003-2293-3525

Eva Stukenbock
Christian-Albrechts University of Kiel and Max Planck Institute for Evolutionary Biology

Eric Kemen
Institute of Plant Biochemistry, ZMBP, University of Tübingen

---

Biological Sciences - Article

Keywords:

Posted Date: January 8th, 2026

DOI: https://doi.org/10.21203/rs.3.rs-8234549/v1

License: This work is licensed under a Creative Commons Attribution 4.0 International License.
Read Full License

Additional Declarations: There is **NO** Competing Interest.

Version of Record: A version of this preprint was published at Nature Microbiology on October 5th, 2026. See the published version at https://doi.org/10.1038/s41564-026-02499-w.

A vitamin cross-feeding mechanism mediates microbial niche adaptation on leaves

Yiheng Hu[1*], Johanna Bode[1], Daniel Gómez-Pérez[1], Marco Alexandre Guerreiro[2,3], Alfredo Mari[1], Kun Wang[1], Sinja Niemann[1], Maryam Mahmoudi[1], Ariane Kemen[1], Paloma Duran[4,5], Oskar Wacker[6], Daniel Straub[6], Sven Nahnsen[6], Benjamin Schwessinger[7], Fabrice Roux[8], Carlos Alonso-Blanco[9], Jon Ågren[10], Stéphane Hacquard[4,5], Eva H. Stukenbrock[2,3], and Eric Kemen[1*]

[1] Department of Microbial Interactions, Centre of Plant Molecular Biology (ZMBP), Eberhard-Karls-University of Tübingen, Tübingen, Germany

[2] Environmental Genomics Group, Botanical Institute, Christian-Albrechts University of Kiel, Kiel, Germany

[3] Max Planck Institute for Evolutionary Biology, Plön, Germany

[4] Department of Plant Microbe Interactions, Max Planck Institute for Plant Breeding Research, Cologne, Germany

[5] Cluster of Excellence on Plant Sciences (CEPLAS), Max Planck Institute for Plant Breeding Research, Cologne, Germany

[6] Quantitative Biology Center (QBiC), University of Tübingen, Tübingen, Germany

[7] Research School of Biology, Australian National University, Canberra, Australia

[8] Laboratoire des Interactions Plantes–Microbes–Environnement, Institut National de Recherche pour l'Agriculture, CNRS, Université de Toulouse, Castanet-Tolosan, France

[9] Departamento de Genética Molecular de Plantas, Centro Nacional de Biotecnología (CNB), Consejo Superior de Investigaciones Científicas (CSIC), Madrid, Spain

[10] Plant Ecology and Evolution, Department of Ecology and Genetics, EBC, Uppsala University, Uppsala, Sweden

*Corresponding authors: Email: yiheng.hu@zmbp.uni-tuebingen.de (Y. H.); eric.kemen@zmbp.uni-tuebingen.de (E. K.)

Abstract:

Microbial homeostasis is crucial for host health and ecosystem function, yet the molecular and ecological mechanisms underlying community assembly and stability remain elusive. Here, we uncover a conserved yeast-oomycete metabolic mutualism that promotes their coexistence in the leaf microbiome. Using a continental-scale microbiome survey, we identified a mutualistic interaction between two eukaryotic hub microbes: the yeast *Dioszegia hungarica* and the obligate oomycete *Albugo laibachii*. We show that *Dioszegia* facilitates *Albugo* colonization by supplying thiamine via a dedicated membrane permease, alleviating *Albugo*'s auxotrophy. Genomic and transcriptomic analyses reveal that natural selection has acted on thiamine production in *D. hungarica*, shaping this mutualistic interaction. *In planta* assays further demonstrate that cross-feeding enhances *Albugo* colonization and promotes *Dioszegia* persistence. Our study illustrates how the evolution of nutrient cross-feeding mediates microbial coexistence and microbiome stability. Targeting microbial nutrient flows offers new strategies for engineering microbiomes and enhancing plant resilience in natural and agricultural systems.

Introduction

Microbial communities play essential roles in shaping host physiology, ecosystem function, and biodiversity[1,2]. The composition of host-associated microbiomes shift across space and time, influenced by environmental conditions, nutrient availability, and host immune activity, which together shape microbial interactions and community dynamics[3,4]. Although host factors are well established as major determinants of microbiome structure and function, which in turn can strongly influence host fitness[1,5,6], microbe–microbe interactions also contribute to assembly and persistence[7]. This question is especially intriguing in transient ecological niches such as perennial plant leaves, known as the phyllosphere, where seasonal fluctuations and abiotic stresses impose strong selective pressures[4]. Despite increasing efforts to characterize microbial interactions in plant leaf microbiomes[8], the molecular mechanisms enabling coexistence, persistence, and community stabilization in such dynamic environments remain largely unresolved.

Hierarchical structures often emerge within plant-associated microbial communities, where certain microbes known as keystone or hub taxa exert a disproportionate influence on community dynamics and stability[9,10]. Microbial interactions, both positive and negative, are central to this process. While negative interactions, such as competition, antagonism and amensalism, contribute to the exclusion or dominance of particular species[11], positive interactions—such as mutualism and commensalism—are especially important for community resilience[12]. Currently, keystone species and their interaction networks are typically inferred from *in silico* predictions[13]. The mechanisms behind microbial interactions and their ecological functions have mostly been validated using synthetic microbial communities *in vitro*[8,12]. Current models of microbiome assembly in plants primarily focus on the metabolic capacities of bacteria and their resource allocations[8]. Despite these advances, it remains unclear which metabolic interactions influence the establishment or shifts in microbial hierarchies in nature, ultimately leading to a stable microbiome. To address this, systems where individual taxa strongly influence community composition offer strategic entry points.

Plant pathogens are well known for their capacity to shape the microbiome[14,16]. In wild *Arabidopsis*, although bacteria are considered the most abundant microbial kingdom[4], the leaf niche is heavily colonized by the obligate biotrophic oomycete pathogen *Albugo laibachii,* which exhibits global prevalence[15,17,18]. Obligate biotrophic oomycetes of the genus *Albugo* have long and complex lifecycles across diverse plant hosts and frequently establish asymptomatic infections in nature[19]. Obligate biotrophic parasites rely on living hosts for nutrients, and can persist for weeks to years on their hosts[20]. This is much longer than necrotrophic or hemi-biotrophic pathogens, which rapidly induce host death. These features suggest that *Albugo* may exert extended ecological influence within the

leaf niche. Consistent with this, our previous work identified *Albugo* as a keystone taxon within the *Arabidopsis* leaf microbiome, showing a high degree of interconnectivity and a strong influence on community structure[21–23]. Therefore, the *Albugo*-centered pathosystem represents an ideal model to study the ecologically relevant mechanism of plant microbiome assembly.

The evolution of obligate biotrophy is often associated with auxotrophy, that is, the loss of essential metabolic pathways such as the biosynthesis of thiamine and molybdopterin[24], since those metabolites can be obtained from the host after successful infection. However, whether members of the microbiome can support auxotrophic obligate biotrophs remains unknown. We hypothesized that specific positive interactions centered around the keystone taxon *Albugo* facilitates niche co-adaptation and long-term persistence *in planta*, ultimately contributing to the hierarchical structure and stability of the broader microbial community. Such sustained positive interactions may form a mechanistic foundation for assembly and homeostasis of stress-resilient plant microbiomes.

Here, we performed a European-scale survey of wild *A. thaliana* leaf microbiomes to identify conserved microbial partners associated with *Albugo*, and uncovered a metabolically mediated mutualistic interaction that likely underpins *Albugo*-driven microbiome assembly in nature.

Results:

A European-scale field survey identifies conserved microbial interactions in the *A. thaliana* phyllosphere

To identify conserved interactions in the *A. thaliana* phyllosphere microbiome, we conducted a continent-scale survey across western, middle and northern Europe to capture the maximum microbial diversity. We collected 347 plants from 15 sites harboring natural *A. thaliana* populations in Spain, France, Germany and Sweden (Fig. 1A). We performed marker gene amplicon sequencing on bacteria (16S), fungi (ITS2), oomycete (ITS1), and other eukaryotes (18S), using half of the plant material as 'whole leaf microbiota' samples and surface-sterilizing the other half to obtain the endophytic-microbiota. Since species-level resolution was not consistently achievable for ITS and 18S markers, and because our goal was to identify conserved ecological structure, we used operational taxonomic unit (OTU) clustering as a harmonized framework for multi-kingdom analysis. Based on OTU classification, we found that microbial alpha diversities (Shannon index) were comparable across different sampling sites (Fig. 1B for endophytes, fig. S1A for whole leaf). However, when we performed principal coordinate analysis, we found that the microbial composition was significantly different at

the genus level (Fig. 1C for endophytes, fig. S1B for whole leaf, Adonis2 $p < 0.0001$). This result agrees with a previous report of host biogeography explaining microbial variation[11,25]. Based on the composition of the microbiome in whole leaf samples (fig. S1C), we found the most abundant taxa to be Alphaproteobacteria among bacteria (53.6%), Agaricomycetes among fungi (15.4%), the genus *Albugo* among oomycetes (57.8%) and Peronosporomycetes among eukaryote microbes (40.3%). We next investigated the intra- and inter-kingdom microbial OTU relationships using the network inference tool Fastspar[26]. Among the major taxa that were primarily shared across different sites (present in > 10 samples, containing minimum 50 reads), we observed a similar number of positive and negative correlations from the whole leaf microbiome (4457 positive and 4075 negative, fig. S1D). To reduce the complexity and focus on the microbes that form tight associations with *A. thaliana*[27], we further constructed a network of endophytes (fig. S1E). To assess the role of each genus in the community, we calculated closeness centrality, quantifying how easily a microbe can reach other microbes within the network, and betweenness centrality, reflecting its bridging influence as a connector in the network[28]. Across all samples, two OTUs classified as *Albugo* appeared to be the major hub-taxa for oomycete and eukaryote OTUs, as reflected by their top ranking in both closeness centrality and betweenness centrality measures of OTUs within their group (Fig. 1D). We also noticed that the yeast *Dioszegia* showed second-highest betweenness centrality among all fungal OTUs. Together with previous evidence suggesting *Dioszegia* as a keystone taxon[29], this finding validated the central positions of *Albugo* and *Dioszegia* within *A. thaliana* leaf microbiome[21].

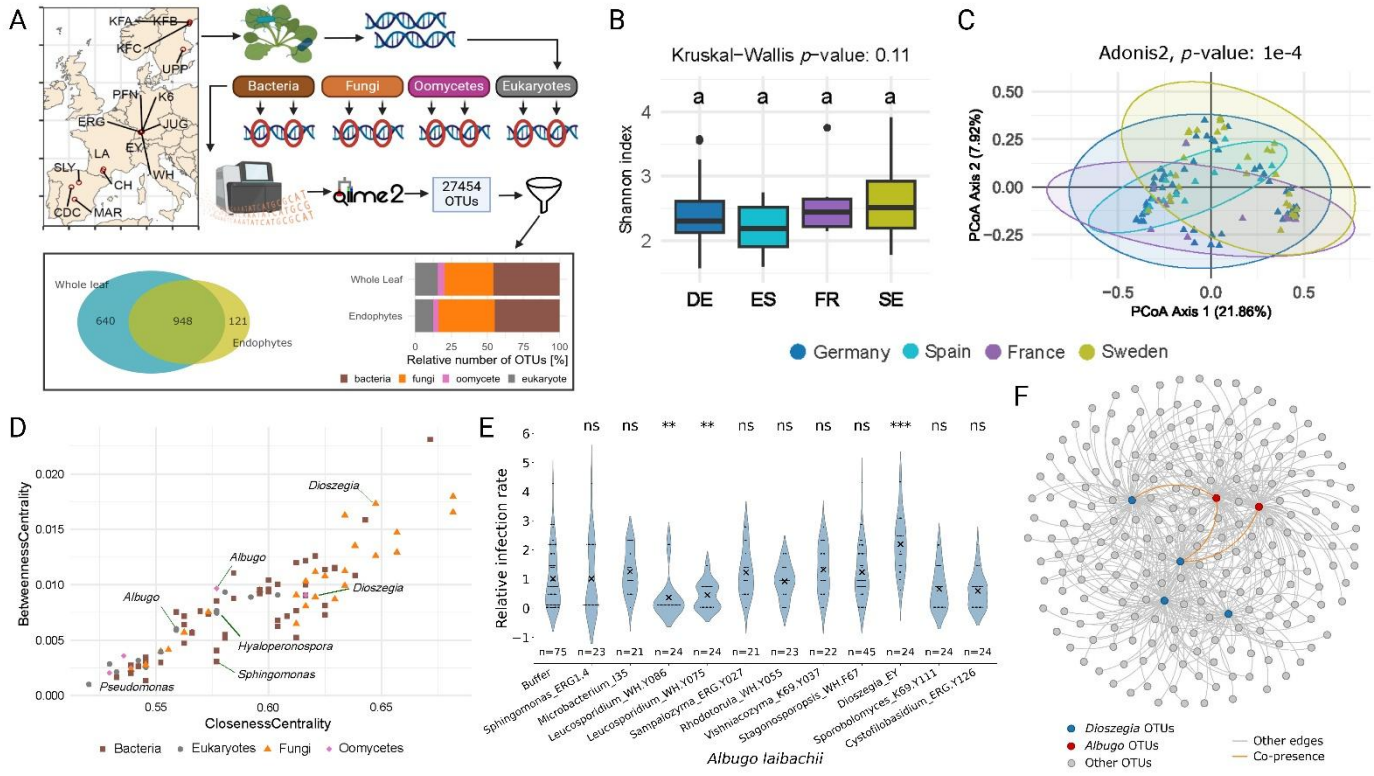


Figure 1. The identification of conserved *Albugo*-*Dioszegia* interactions from a European-scale survey of *A. thaliana* phyllosphere microbiome.
(A) The workflow of field sampling and overview of the whole leaf and endophyte dataset about the relative OTU numbers of each taxa group and overlapping OTUs. (B) Alpha-diversity of endophytic samples from different countries measured by Shannon index. Letters depict insignificant differences across countries (p=0.11, Kruskal-Wallis test). (C) Principal coordinate analysis (PCoA) based on Bray–Curtis distances between endophytic samples from different countries. Each color represents all samples from the same country. (D) Measures of closeness centrality and betweenness centrality of the endophytes OTUs. Only OTUs present in at least 10 samples and containing a minimum of 50 reads were retained for downstream analyses. OTUs belonging to the same species were combined and only genus names are displayed. (E) Violin plot showing *Albugo laibachii* infection rate relative to the buffer control when co-inoculated with different interactor strains (mainly basidiomycete yeasts). The common environmental yeasts *Rhodotorula* and *Cystofilobasidium* isolate were not among the interactors and were used as negative controls. The infection rate of each group is calculated based on the average number of infected leaves per plant at 12 days after *Albugo* inoculation (dai, see supplementary methods), and normalized to the buffer control of each experiment. The X in the violin plots represents the mean of each dataset. Asterisks or ns represent the p value from Mann-Whitney U test between each treatment group and the buffer control. ***p < 0.001, **p < 0.01, *p < 0.05, or ns: p >=0.05. (F) Co-abundance network subset from the whole leaf network, containing only *Albugo* and *Dioszegia* OTU nodes and their direct interactors. Red and blue nodes represent *Albugo* and *Dioszegia* OTUs, respectively; orange edges between them represent positive interactions based on co-presence in the network.

A basidiomycete yeast *Dioszegia* strain promotes the colonization of *A. thaliana* by *A. laibachii* under gnotobiotic conditions

Given *Albugo's* central role in the microbial network, we hypothesize that its direct interactions with other microbes play a key role in the assembly of the *Arabidopsis* leaf microbiome. To investigate this, we ranked both predicted positive and negative interactions involving *Albugo* OTUs in the whole leaf samples based on the crossness and betweenness centrality measures (table S1), and attempted to experimentally verify these interactions to unravel the molecular mechanisms of *Albugo*-centered microbial interactions. We adapted a previous gnotobiotic system using sterile *A. thaliana* grown on 12-well plates to screen and quantify the effect of single phyllosphere microbes on the colonization of *Albugo laibachii*. We assessed colonization success based on number of infected leaves per plant and qPCR quantification of *Albugo* biomass (fig. S2A). Using this system, we tested 12 potential *Albugo* interactors. These interactors are identified from our inferred network, and correspond to taxa that had been previously isolated from wild *A. thaliana* near Tübingen (48.45N, 8.78E). We found that most of the *Albugo*-interacting microbes were either pathogenic to *A. thaliana* or had no effect on *A. laibachii* infection (Fig. 1E, fig. S2B). In addition, an OTU classified as the basidiomycete yeast *Leucosporidium* was predicted to form a strong positive interaction with *Albugo* (table S1), but different strains of this genus significantly inhibited *Albugo* infection under gnotobiotic conditions (Fig. 1E). This result indicated that the pairwise microbial interactions from the network can be context-dependent and shaped by environmental factors[30,31], leading to deviations from experimental outcomes. In contrast, *Dioszegia* EY consistently showed a positive interaction with *A. laibachii*, aligning with *in silico* predictions (Fig. 1E). The basidiomycete yeast *Dioszegia* was identified as a major

hub-taxon in the *A. thaliana* phyllosphere microbiome in our previous study[21] and was among the most interconnected fungal OTUs with the second highest betweenness centrality in the present study (Fig. 1D). When we subset the whole leaf network and separated all direct interactions of *Albugo* and *Dioszegia* OTUs, we observed three direct interactions between the two *Albugo* OTUs and two *Dioszegia* OTUs, while two other *Dioszegia* OTUs had indirect interactions with *Albugo* OTUs (Fig. 1F). The results from both *in silico* and *in planta* experiments suggest that the positive interaction between *Albugo* and *Dioszegia* represents a key microbial interaction in the phyllosphere microbiome of different *A. thaliana* populations.

Comparative genomics identifies a *D. hungarica* thiamine permease that is crucial for the *Dioszegia-Albugo* interaction

Many biotrophic microbes, including *A. laibachii*, have lost several essential but energetically costly metabolic pathways throughout evolution and have become auxotrophic for thiamine, molybdopterin, and a few other essential metabolites[24]. *A. laibachii* can acquire essential nutrients from host cells through haustoria upon successful penetration of the plant leaf. However, this process is limited during the early infection stage on the leaf surface, which is a challenging environment with limited resources for microbes[31,32]. Therefore, we hypothesized that the metabolic auxotrophy of *Albugo* may be complemented by positive interactors such as *Dioszegia*.

We employed comparative genomics to identify genetic differences between *Dioszegia* strains that promote and those that do not promote *Albugo*, focusing on essential metabolic pathways absent in *Albugo*. We first obtained nine strains of *Dioszegia* from the fungal collection center in the Netherlands (table S2) and tested their influence on *A. laibachii* infection. We observed that *Dioszegia* strain CBS10163 (PT), originating from maple leaves in Portugal, did not promote *A. laibachii* infection (Fig. 2A). We next generated draft genomes of *Dioszegia* EY and PT strains using a recent reference[33] (table S3) and compared all their thiamine related genes as a natural first choice. We found seven functional groups for a total of 14 thiamine-related genes in each genome and manually curated them by RT-PCR and Sanger sequencing. To characterize genetic variation of these 14 genes, we compared the number and distribution of the single nucleotide polymorphisms (SNPs) for each thiamin-related gene between *Dioszegia* EY and PT strains. We observed that one gene (*DhPER1*, 105.7 SNPs/kb) has a high density of SNPs relative to the other thiamine-related genes in EY and PT genomes (Fig. 2B), nearly doubled that of the second highest genes. *DhPER1* also carries the highest amino acid variation of all five permease genes (fig. S3A), possibly resulting in functional diversification.

We also inspected *in vitro* transcriptional differences related to thiamine metabolism between the two strains *in vitro*. *DhPER1* expression was more than 20-fold higher in *Dioszegia* EY than in PT (Fig.

2C), and was the only thiamine-related gene with negligible expression in PT (fig. S3B). The expression difference might be related to high levels of nucleotide diversity in the extended promoter region (2 kb upstream) of the coding sequence (fig. S3C), suggesting that this expression difference is due to *DhPER1 cis*- and/or *trans*-regulatory mutations. To determine whether *DhPER1* is the primary permease for thiamine, we predicted protein structures of all five permeases and aligned them with the predicted structure of a known thiamine transporter, *THI7*, from *Saccharomyces cerevisiae*[34] (fig. S3D). Based on three structural similarity metrics—percentage identity, root mean square deviation (RMSD), and template modeling (TM) score—DhPER1 was one of the two closest matches to THI7. We also performed molecular docking of DhPER1 with thiamine-HCl, the transportable form of thiamine, and thiamine-HCl anchored well with the predicted protein (Fig. 2D). Comparison of *DhPER1* protein structure and molecular docking with thiamine-HCl between EY and PT predicted proteins did not show significant structural differences (fig. S3E&F). Therefore, although both structural and regulatory polymorphisms in *DhPER1* might affect its function, the low predicted impact of missense mutations and the near absence of expression in *Dioszegia* PT suggest that the differential expression of *DhPER1* in *Dioszegia* EY underlies its beneficial effect on *Albugo* colonization of *A. thaliana* leaves.

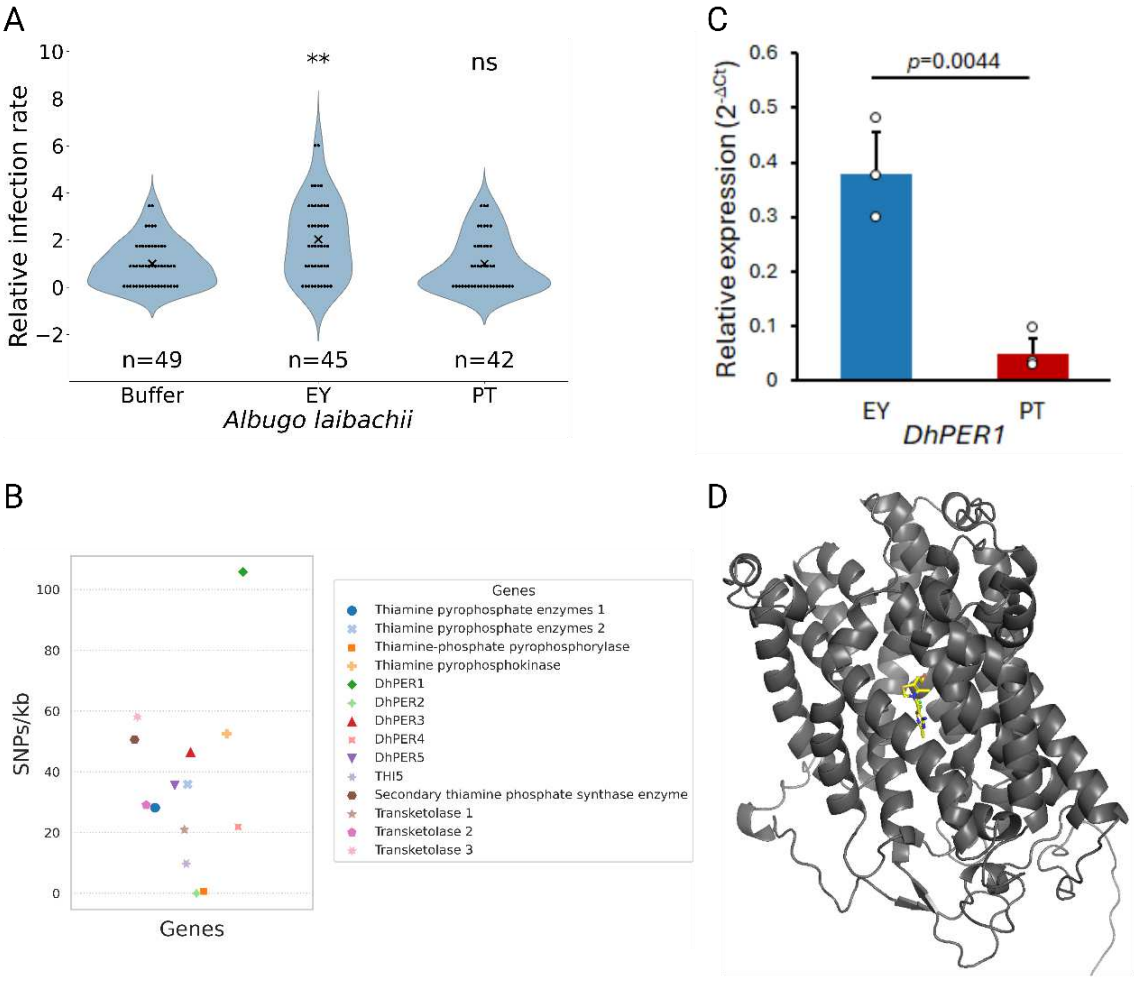


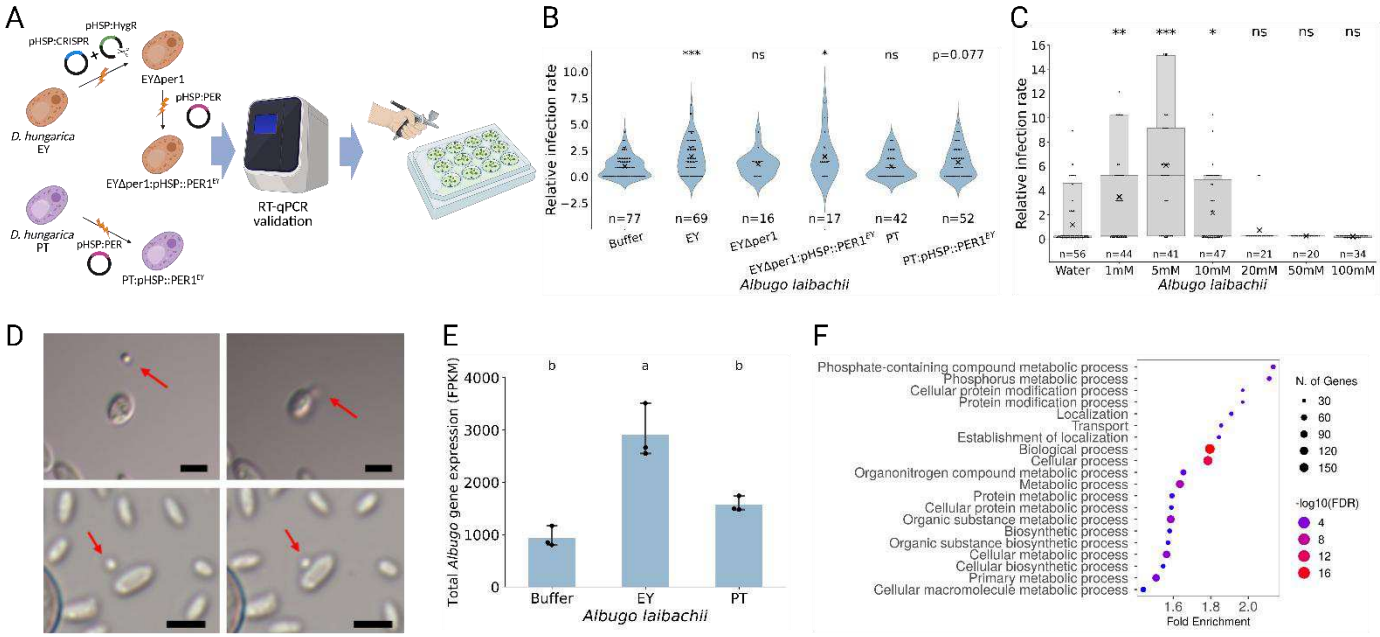
Figure 2. A thiamine permease is differentially expressed in *A. laibachii* promoting and non-promoting strains of *Dioszegia*.
(A) Violin plot showing the infection rate (number of infected leaves per plant at 12 dai) of *A. laibachii* in the presence of either *Dioszegia* EY or PT as normalized to buffer control. X represents the mean of each dataset. Asterisks or ns represent the *p* value from a Mann-Whitney U test between each treatment group and the buffer control. ***p*=0.0018, or ns: *p*=0.69. This experiment was replicated more than three times and the same result was observed. (B) Scatter plot illustrating the variations of coding sequences (CDS) of all thiamine metabolism genes between PT and EY. The variations are shown as SNPs/kilo basepairs. (C) Quantitative RT-PCR results measuring the relative expression of *DhPER1* between EY and PT *in vitro*. The expression of *DhPER1* is normalized to the expression of *D. hungarica* elongation factor 1α (*EF1*α) gene. Each data point was calculated from the median of three technical replicates. *p* value was calculated using Student's t test. (D) Molecular docking of the thiamine-HCl compound with *DhPER1* (grey color in ribbon representation) from *Dioszegia* EY using DiffDock (https://github.com/gcorso/DiffDock).

The *DhPER1*^{EY} is responsible for thiamine-mediated *A. laibachii* promotion *in planta*

We sought to confirm the genetic and functional importance of *DhPER1* in *A. laibachii* promotion. We developed an electroporation-based transformation and CRISPR system for the *Dioszegia* EY strain (Figure 3A). We identified a mutant (EYΔper1) with a 389 bp insertion in the first intron of *DhPER1*, which abolished the expression of *DhPER1*^{EY} (fig. S4A&B). We complemented the EYΔper1 mutant and subsequently tested the mutant and complemented strains in the gnotobiotic system with *A. laibachii*. Both phenotyping and qPCR analyses revealed that the EYΔper1 mutant had lost its capacity to promote *Albugo* infection, while complementation of the mutant with *DhPER1*^{EY} under a heterologous overexpression promoter restored the phenotype (Fig. 3B, fig. S4C&D). We also ectopically expressed *DhPER1*^{EY} in the PT strain using the same overexpression promoter (fig. S4E). We found that PT overexpressing *DhPER1*^{EY} facilitated *Albugo* infection slightly, but the effect was not significant (Student's t-test, *p*=0.077, Fig. 3B). This result suggests that the differential expression of *DhPER1*^{EY} between *Dioszegia* EY and PT strains is necessary but not sufficient to fully promote *Albugo* infection. We also transformed PT with *DhPER1*^{EY} under EY's endogenous promoter, and the transformant did not increase *DhPER1* expression (fig. S4E). Hence additional *trans*-regulation on *DhPER1* expression also differentiates between *Dioszegia* EY and PT strains. Together, these results indicate that *DhPER1* is a key *Dioszegia* gene responsible for *Albugo* promotion, and *Dioszegia* PT strain lacks multiple genetic components of the *DhPER1* pathway mediating the facilitation of *Albugo* infection.

Next, we attempted to validate the metabolic and physical basis of interactions between *Dioszegia* and *Albugo*. To avoid priming the plant by applying first thiamine and then *Albugo*, we applied different concentrations of thiamine together with *A. laibachii* in the gnotobiotic system[35]. We found that low concentrations of thiamine increased the success of *A. laibachii* infection by up to 500% (at 5mM, Mann-Whitney U-test *p*=2.8e-08) as compared to the buffer control (Fig. 3C). The promotion effect sharply dropped when the thiamine concentration was higher than 10mM and thiamine became lethal to the plants from 20mM (Fig. 3C). To test whether thiamine-mediated infection promotion

277 resulted from direct *Dioszegia-Albugo* interaction, we applied *A. laibachii* spores on *Dioszegia* EY cell
278 clumps and tracked the movement of hatched zoospores under the microscope. We observed that
279 once zoospores were physically close to *Dioszegia* EY cells, they moved in the direction of EY cells
280 instead of moving freely in water (Movie S1-S6). These results support the hypothesis that *Dioszegia*
281 EY attracts *A. laibachii* zoospores and cross-feed thiamine to the zoospores via physical contact.



282 **Figure 3. Positive feedback cycle between *Dioszegia* EY and *Albugo* depending on *DhPER1*.**
283 (A) Overview of the strategy for the genetic modification of *Dioszegia* EY and PT strains. The expression of
284 *DhPER1*^{EY} was first validated in all the five strains depicted through RT-qPCR, followed by *in planta* testing using
285 the gnotobiotic infection system. (B) Violin plot showing the infection rate of *A. laibachii* in the presence of
286 different *Dioszegia* EY and PT strains normalized to the buffer control. The EYΔper1:pHSP::PER1^{EY} represents the
287 complementation strain of the EYΔper1 mutant, and the PT:pHSP::PER1^{EY} represents the PT complementation
288 strain with overexpressing *DhPER1* gene of EY. (C) Boxen plot showing the effect of different concentrations of
289 thiamine on *A.laibachii* infection, quantified by the relative infection rate. The bottom dark grey boxes represent
290 the 50% percentile and the upper light grey boxes represent 75% percentile. X in (B) and (C) represent the mean
291 of each dataset. Asterisks or ns in (B) and (C) represent the *p* value from Mann-Whitney U test between each
292 treatment group and the buffer control. ***$p < 0.001$, **$p < 0.01$, *$p < 0.05$, or ns: $p >= 0.05$. (D) Light microscopic
293 images show an *A. laibachii* zoospore before (left panel) and after (right panel) attaching to *D. hungarica* cells
294 (EY). Both events have associated videos to illustrate the attaching process (Movie S1-S6). Scale bar: 5 µm. (E)
295 The total expression patterns of *A. laibachii* at 2 dai measured by FPKM. The samples are from sterile plants
296 sprayed with *A. laibachii* and *Dioszegia* EY or PT, and harvested at 2 days after infection (2 dai). The different
297 letters represent significant difference from Tukey's HSD test results (p<0.01). (F) Dot plots showing the term
298 enrichment (GO: Biological Process) analysis on all *A. laibachii* DEGs upregulated by *D. hungarica*. Top 20
299 enriched GO terms displayed, ranked by fold enrichment.

300 The release of zoospores is the very first step of oomycete infection[36]. To verify our hypothesis, we
301 used an RNA-seq approach to test whether adding *Dioszegia* would promote the infectivity of *Albugo*
302 zoospores. We sprayed *A. laibachii* with either *Dioszegia* EY or PT, or a buffer-only control on sterile
303 *A. thaliana* leaves, and collected samples for total RNA-seq two days after infection (dai). Sequencing
304 produced mixed plant–microbial transcriptomes, which we mapped simultaneously to the *Arabidopsis*
305 and *Albugo* reference transcriptomes. Reads assigned to the *Albugo* transcriptome were extracted to

quantify pathogen activity using fragments per kilobase per million mapped reads (FPKM). Total *Albugo* expression increased threefold in the presence of *Dioszegia* EY compared to the buffer control (Tukey's HSD test $p<0.001$), whereas *Dioszegia* PT had no significant effect (Fig. 3E). A principal coordinate analysis of the gene expression data revealed distinct expression patterns among the three groups (fig. S5A). Using $|\log_2 FC| \geqslant 1$ and false discovery rate (FDR) < 0.05 cut-offs, we identified 316 differentially expressed genes (DEGs) in *A. laibachii* when infected plants were sprayed with *Dioszegia* EY compared to the buffer control, all of which were upregulated (fig. S5B). In contrast, PT treatment upregulated only 20 *A. laibachii* genes, all of which were also present in the EY-induced DEGs (fig. S5C). Gene ontology (GO) term enrichment analysis of the 316 upregulated *A. laibachii* genes showed an overrepresentation of terms related to metabolic processes and membrane transport (Fig. 3F, fig. S5D&E). Thus, the transcriptome analysis showed that *Dioszegia* EY treatment induced *Albugo* metabolism during the early stage of infection, facilitating initial colonization of *A. thaliana* by *Albugo*. Together, our results demonstrate that *DhPER1*^{EY} mediates thiamine cross-feeding from *Dioszegia* EY to *A. laibachii*, supporting its establishment.

Genetic rearrangements and translational optimization at the *Dioszegia PER1* locus

How did this natural cross-feeding mechanism evolve, and how did *DhPER1* differences between *Dioszegia* EY and PT arise? We addressed these questions by comparing the gene sequences of thiamine-related genes, and we investigated patterns of transcription and translation. We first examined evidence of selection on *DhPER1* by comparing the dN/dS ratio with all other genes families. We collected different *Dioszegia* strains either from *A. thaliana* near Tübingen, and included also different type strains available from the fungal collection center in our comparisons. In addition to the four available *Dioszegia* genomes[33,37,38], we generated draft genome assemblies for 10 *Dioszegia* strains (table S3) and queried homologous genes to *DhPER1*. We identified *DhPER1* orthologs from seven *Dioszegia* genomes comprising four species (fig. S6A). We aligned the predicted proteomes from all *Dioszegia* strains and mapped their coding sequences (CDS) to the protein alignment before modelling the dN/dS ratio for all genes. The results indicate that *DhPER1* is under strong purifying selection with a dN/dS ratio of approximately 0.05 (top 5% conserved across all genes) in all *Dioszegia* strains that carry it (Fig. 4A). We also investigated the diversification of *DhPER1* within the fungal kingdom. We identified putative orthologs for this gene in 171 fungal species using the NCBI non-redundant protein database. We then constructed a phylogenetic tree (fig. S6B) and assess whether there was any evidence of selection during the diversification of this thiamine permease. Using the Relaxed Selection test[39], We observed that this gene has been subject to variable levels of selection across its genealogy, including both relaxed and intensified, with the *Dioszegia* branch showing

significantly increased purifying selection on this gene (fig. S6C). The evidence for intensified selection further increased when considering exclusively the *D. hungarica* branch. *Dioszegia* is an environmental yeast genus with global distributions[40]. The conservation and strong selection on *DhPER1* indicate the importance of the thiamine transporter function for the survival of *Dioszegia* within the niche of *A. thaliana* leaves, likely influenced by *Albugo*.

To further investigate the selection of *DhPER1* differential expression between *Dioszegia* EY and PT, we compared a 100 kb region around the *DhPER1* gene. We found several gene duplications, structural and copy number variations within this region, indicating active chromosomal rearrangements (Fig. 4B). Since chromosome rearrangements are known to be associated with altered gene expression[41], we performed a long read RNA-seq experiment from pure EY and PT cultures to assess the gene expression changes at this locus. *Dioszegia* EY showed overall increased gene expression in this region, as eight genes showed increased expression more than one-fold compared to PT, including four genes that increased more than 10-fold (Fig. 4B). Only two PT alleles showed increased expression in this region, both less than three-fold. In contrast, another permease gene (*DhPER2*) resides in a less variable region, wherein most genes in this region did not show large variations in expression (fig. S6D).

In addition to changes in amino acid sequences and gene expression, natural selection may also act at the level of protein translation. To explore the impact of selection on translation in the mutualistic *Dioszegia* strain, we investigated codon usage across the genome. Specifically, we asked whether *Dioszegia* EY optimized its translational machinery correlated with the cross-feeding mechanism. We first screened the tRNA gene content of all four *D. hungarica* genomes, and found that the *Dioszegia* EY genome encodes a total of 137 tRNA genes, more than twice that of all other strains (Fig 4C). The excess tRNA genes of *Dioszegia* EY span a total of 10 amino acids, with the methionine-encoding start codon showing the highest difference compared to the number of methionine-encoding tRNA in all other *D. hungarica* genomes (fig. S7A). We also compared the relative tRNA composition and codon usage bias which are largely similar among all four *D. hungarica* genomes (fig. S7B). Previous studies have shown that the copy number of tRNA genes in the genome correlate with tRNAs abundance in the cytoplasm[42,43], and that the initiation of translation is the limiting step[44]. With similar codon usage but a higher number of tRNA genes, our results indicate that *Dioszegia* EY can achieve higher protein translation rates compared to other strains, especially during the start of translation.

To determine if these translational adaptations influence thiamine-related genes, we inferred the intensity of translational selection on the thiamine metabolism genes between *Dioszegia* EY and PT using the codon optimization index (S). S is based on the tRNA gene pool, codon usage bias and the effective number of coding codons[45,46]. We found that the S indices of the complete sets of CDS were

similar between EY and PT genomes, and the thiamine-related genes had more than twice as high S indices compared to all other CDS (Fig. 4D), suggesting significant translational optimization in *D. hungarica* thiamine-related genes. We further validated the codon optimization analysis by assessing translation efficiency using a tRNA adaptation index (tAI), measuring the co-evolution between a given CDS and the respective genome tRNA pool[45,47]. We found that the normalized tAI of all thiamine-related genes is not significantly different between EY and PT, but the tAI of *DhPER1* is higher in EY (Fig 4E, table S4), indicating translational optimization correlated with the cross-feeding mechanism. Taken together, our results indicate that *Dioszegia* EY strain has experienced selection for an optimized translation of thiamine related genes, especially *DhPER1*, suggesting that adaptation of *Dioszegia* EY to the leaf environment has involved regulation of the cross-feeding mechanism.

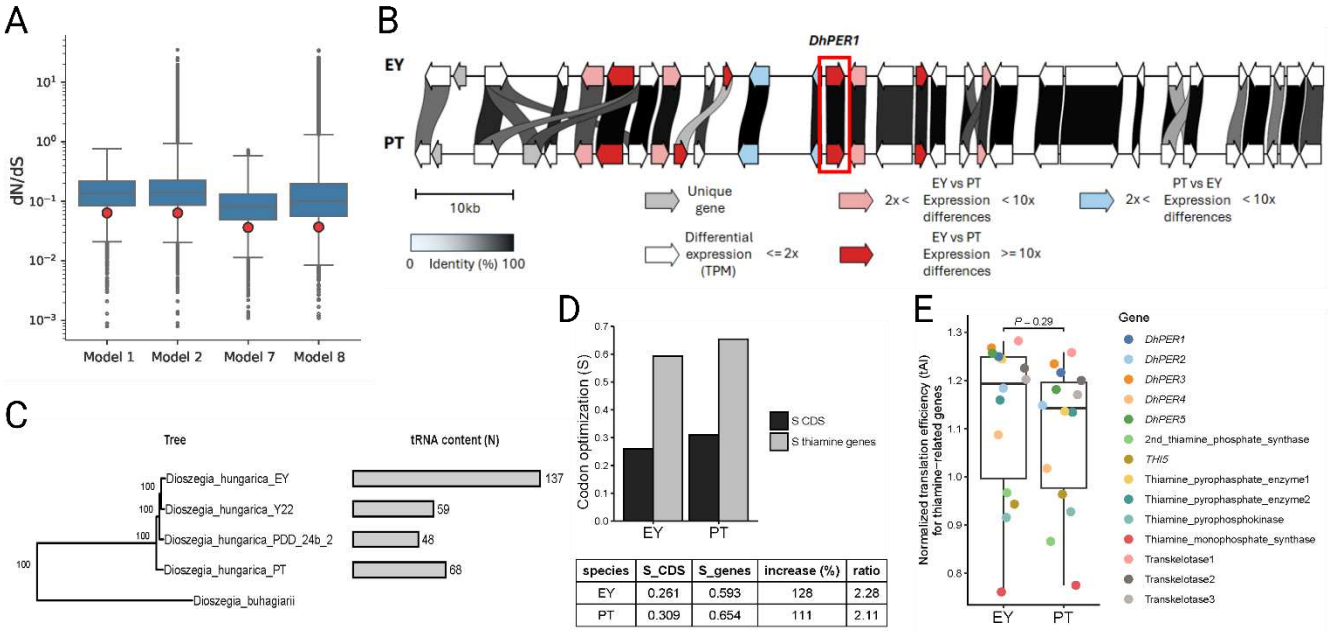


Figure 4. Evidence for selection of the *DhPER1*-driven cross-feeding mechanism.
(A) Evaluation of the conservation of *PER1* orthologs from all seven *Dioszegia* genomes carrying permease using phylogenetic analysis by maximum likelihood (PAML). The x-axis represents different models of dN/dS analysis used by the program. Models 1 and 7 are null models, and models 2 and 8 allow for positive selection. Red dots indicate purifying selection (dN/dS close to 0) ratio of *DhPER1* under each model. (B) Global alignment of the 100kb *DhPER1* region using clinker[48]. Only paralogues with greater than 35% amino acid identity (%) were annotated with linker. The color of each gene represents the transcriptional differences between each paralogue within this region. (C) tRNA content of each *D. hungarica* genome. The phylogeny is based on whole genome alignment using *Dioszegia buhagiarii* genome as outgroup. (D) Comparison of codon optimization index S between thiamine-related genes and the whole genome CDS. The table below shows increased S index in *Dioszegia* EY and PT's thiamine-related genes compared to their own whole genome S index. (E) Comparison of the translation efficiency between EY and PT's thiamine-related genes measured via the tRNA adaptation index (tAI) normalized to the mean tAI of the whole genome CDS. *p* value is calculated using Student's t-test.

DhPER1^{EY} facilitates the long-term survival of *Dioszegia* with *Albugo*

Thiamine is an expensive but essential nutrient to synthesize, so what is the selective advantage to *Dioszegia* of this mechanism? Many *in vitro* studies have shown that microbes produce 'public goods' - metabolic products that are costly to produce but benefit individuals in shared environments

independently of species[12,49,50]. Additionally, synthetic ecology experiments suggest that this lifestyle promotes long-term stability and stress resilience of the public-good producer in a community, especially under transient environmental conditions[12]. To examine this idea, we designed a long-term experiment, in which *Albugo* was co-cultivated with *Dioszegia* EY, PT, EYΔper1 mutant or complementation strains EYΔper1:pHSP::PER1^{EY} and PT:pHSP::PER1^{EY}, to track the *Dioszegia* population over most of *A. thaliana's* vegetative growth stage (Fig. 5A). First, to investigate whether *Dioszegia* EY and PT can successfully colonize *A. thaliana* leaves, we assessed their growth in both gnotobiotic and holoxenic (plants grown on non-sterile soil) conditions without *Albugo* at different time points (12, 20 and 32 dai). Interestingly, both *Dioszegia* EY and PT colonized well under gnotobiotic conditions, whereas their populations gradually became extinct in the presence of an endogenous microbiome under holoxenic condition (Fig. 5B). This result indicates that it is difficult for *D. hungarica* alone to persist in an *Albugo*-free community.

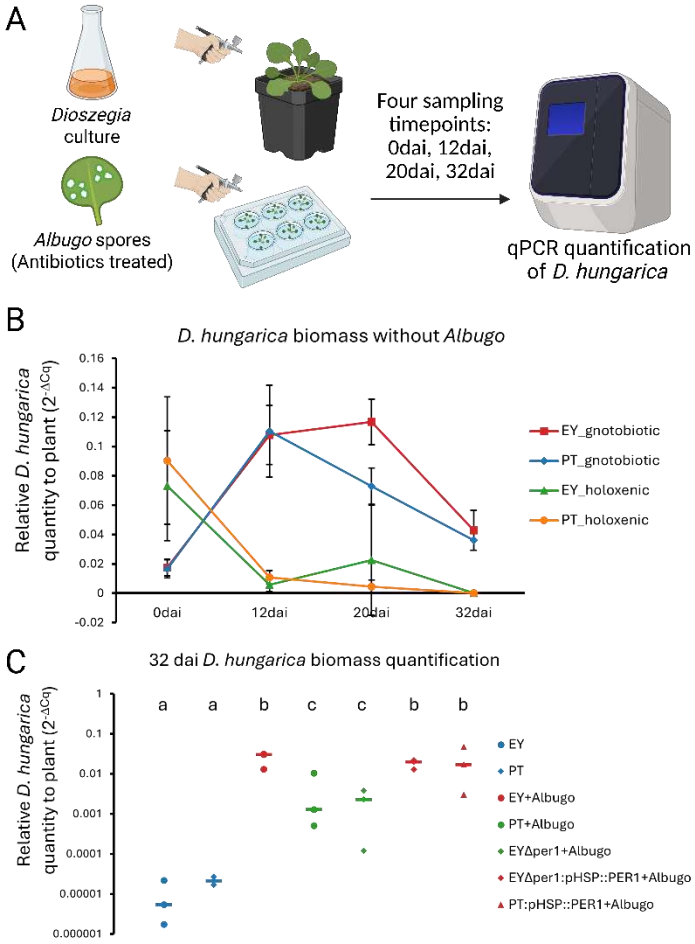


Figure 5. The ecological impact of the cross-feeding mechanism in a lab environment.
(A) Workflow of the long-term co-cultivation experiment. (B) Biomass of *Dioszegia* EY and PT strains under gnotobiotic and holoxenic conditions during a 32-day time course without *Albugo*. qPCR analysis was used for biomass quantification. Each data point shows the mean ± standard error of *Dioszegia* biomass from 3 plants, and each plant sample contains three technical replicates. (C) Biomass of different *Dioszegia* strains under holoxenic conditions at 32 dai. Different colors represent different experiment groups (*-Albugo*, *+DhPER, -DhPER*). Different letters represent significant differences in effect size between groups (Cohen's d > 0.8). In both (B) and (C) the *DhEF1a* gene is used for qPCR and normalized to the *EF1a* gene from *A. thaliana.*

In the presence of *Albugo*, the *Dioszegia* population stabilized over the growing period under both conditions: not only did the biomass change more slowly, but also the standard deviation in all treatment groups was lower in the later sampling dates as compared to earlier sampling dates (fig. S8B&C). Based on the results from both conditions, we believe that the 32 dai timepoint in the growth chamber best reflects the long-term stability of different *Dioszegia* strains. Interestingly under holoxenic condition, *Albugo* infection 'rescued' *Dioszegia* from extinction and increased its population by more than 100-fold (Fig. 5C, fig. S8C). The populations of *Dioszegia* strains expressing *DhPER1* (EY, EYΔper1:pHSP::PER1^{EY}, PT:pHSP::PER1^{EY}) were significantly larger compared to *DhPER1* non-expressing strains (EYΔper1, PT Cohen's d > 0.8). In contrast, we did not observe the same beneficial effects on *Dioszegia* under gnotobiotic conditions where the microbial interaction is primarily pairwise between *Dioszegia* and *Albugo* (fig. S8B). In this condition, *Albugo* quickly overtook and restricted the growth of all *Dioszegia* strains throughout the colonization period. These results align with results from previous *in vitro* microbial ecology study[12], and indicate that thiamine cross-feeding is crucial for the long-term stability of *Dioszegia* with *Albugo*. However, this benefit is evident only within complex microbial communities where strong competition is present among community members.

Discussion

Our study identified two prevalent hub microbial taxa from natural *A. thaliana* leaf microbiome that interact and have adapted to each other in nature via vitamin cross-feeding (fig. S9), with the basidiomycete yeast *Dioszegia* investing in surplus thiamine production and secretion to facilitate the colonization of the other hub taxon *Albugo*. In return, *Albugo* establishes an environment conducive to the long-term survival of *Dioszegia*. The persistent co-existence of *Albugo*'s across the life cycle of *A. thaliana* further stabilizes the microbiome over time[19]. Combined with our previous work showing that *A. laibachii* creates niches by selectively suppressing certain microbes within the microbiome[22], we propose that the *Albugo*-centered interaction network is a fundamental component of *A. thaliana* leaf microbiome assembly and stabilization. Our work complements recent studies focusing on within-microbiota competition[51,52], providing an integrated view of molecular mechanisms behind the regulation of microbiome assembly by key microbes. In the context of the host-associated microbiome, a majority of microbial cooperations are associated with nutrient exchange, such as the arginine exchange in the human gut[53], and the carbon exchange between bacteria and arbuscular mycorrhiza fungi[54]. These findings underscore the significance of such mutualistic interactions in mediating microbiome stability and support the hypothesis that nutrient-driven co-dependencies are key drivers of microbiome assembly and sustainability[8].

Signatures of selection in *DhPER1* and other thiamine-related genes suggest adaptive specialization in basidiomycete yeasts supplying public goods in *A. thaliana* leaves. The observed adaptation in *Dioszegia*, together with the loss of key biosynthetic functions in *Albugo,* aligns with the 'Black Queen Hypothesis', in which leaky public goods drive stable metabolic dependencies[55]. Although this framework has been applied predominantly to bacterial systems, our results demonstrate that analogous gene-loss–driven resource sharing can also structure eukaryotic microbial interactions. Consistent with this interpretation, co-cultivation experiments showed that *Dioszegia* establishes only under gnotobiotic conditions and is restricted by the native microbiome (Fig. 5B), suggesting that its evolutionary trajectory is shaped primarily by microbial interactions rather than host influence. Moreover, the presence of *A. laibachii* increased the abundance of *Dioszegia* strains lacking *DhPER1*^{EY} during long-term co-cultivation (Fig. 5C). In line with previous studies[52,53], this result indicates that the interaction network extends beyond a single gene-loss dependency and likely involves multiple microbial partners and layered ecological functions. This interaction complexity opens an intriguing area of fundamental research, highlighting the needs to combine computational and experimental approaches to fully understand the direct metabolic interactions within microbiome.

Vitamin auxotrophy is a crucial feature in bacterial communities across various environments, including plants, oceans, and the human gut, and considered a driving force in community stability[56–59]. However, in plant-associated obligate microbes, such as rusts, powdery mildews and arbuscular mycorrhizal fungi, nutrient auxotrophy is primarily regarded as a host-dependent trait, despite their central roles in both leaf and root microbiomes. Previous studies observed that auxotrophic microbes can only store nutrients sufficient for a few population doublings[57]. Given that the successful colonization of *Albugo* and other obligate microbes can take weeks to months[36,60,61], these microbes require a steady nutrient supply beyond what is available for just a few population doublings to successfully reach their hosts. Combined with our findings on the *Albugo-Dioszegia* mutualism, we speculate that the colonization of obligate biotrophic microbes might be functionally dependent on auxotrophic nutrients from the microbiome, not only from the host. Further exploration of this concept could lead to novel strategies to manage obligate plant pathogens or symbionts by harnessing microbiome-originated nutrient supplies, thereby enhancing disease management and promoting crop production.

Data availability:

All raw data was uploaded into NCBI short read archive under Bioproject PRJNA1190083 and are available at the following URL: https://www.ncbi.nlm.nih.gov/bioproject/PRJNA1190083. The

accessions for each genome generated in this study were summarized in table S3. All scripts for data analysis and figure plotting were deposited at https://gitlab.plantmicrobe.de/yiheng/thiaminecrossfed/. The folders referred in the Materials and Methods are all under this repository. All scripts and source data for figures plotting were stored in /Scripts_for_data_analysis_and_figure_plotting/scripts_for_figure_plotting/ if not otherwise indicated in the method.

Acknowledgements

We thank Dr. Libera Lo Presti, Prof. Jeffery L. Dangl and Prof. John P. Rathjen for critical reading of the manuscript. We also acknowledge Prof. Detlef Weigel, Dr. Sangtae Kim, Dr. Rebecca Schwab, and Ms. Martina Kolb for sharing sampling sites and providing support near Tübingen. Special thanks go to Ms. Elke Klenk, Ms. Charlotte Kirn, Ms. Hannah Gall, Ms. Viviane Sevinc and Ms. Aleksandra Placzek for their technical assistance, and to Dr. Bilal Ökmen for sharing plasmids. We further acknowledge the de.NBI Cloud Storage and bwForCluster BinAC Tübingen for providing resources for data storage and analysis. All illustration figures were created using BioRender.com.

Funding:

E.K.: European Research Council (ERC) under the DeCoCt research program (ERC-2018-COG 820124), the Deutsche Forschungsgemeinschaft (DFG) excellence strategy-EXC 2124–390838134, and the TRR356 PlantMicrobe program from the DFG.

Y.H.: University of Tübingen Promotion of Junior Researcher project: PRO-HU-2023-07

S.H.: ERC Consolidator Grant MICROBIOSIS

C.A.-B.: Grant PID2022-136893NB-I00 from the MCIN / MCIU / AEI / 10.13039/501100011033.

J.A.: The Swedish Research Council grants 2016-05435, 2020-04434.

Author contributions: Biological discovery and conceptualization: Y.H., E.K.; Computation: Y.H., J.B., M.M., D.G., M.G., E.H.S.; Experiments: Y.H., A.M., K.W., S.N., A.K.; Methodology: Y.H., A.M., J.B., M.M., D.G., M.G., A.K., C.A.-B., J.A., F.R.; Writing: Y.H., J.B., D.G., M.G., S.H., E.H.S., B.S., C.A.-B., J.A., F.R., E.K.

Competing interests: The authors declare no competing interests.

Reference

1. Lynch, J.B., and Hsiao, E.Y. (2019). Microbiomes as sources of emergent host phenotypes. Science *365*, 1405–1409. https://doi.org/10.1126/science.aay0240.

2. Van Der Heijden, M.G.A., Bardgett, R.D., and Van Straalen, N.M. (2008). The unseen majority: soil microbes as drivers of plant diversity and productivity in terrestrial ecosystems. Ecology Letters *11*, 296–310. https://doi.org/10.1111/j.1461-0248.2007.01139.x.

3. Coyte, K.Z., Schluter, J., and Foster, K.R. (2015). The ecology of the microbiome: Networks, competition, and stability. Science *350*, 663–666. https://doi.org/10.1126/science.aad2602.

4. Vorholt, J.A. (2012). Microbial life in the phyllosphere. Nat Rev Microbiol *10*, 828–840. https://doi.org/10.1038/nrmicro2910.

5. Wilde, J., Slack, E., and Foster, K.R. (2024). Host control of the microbiome: Mechanisms, evolution, and disease. Science *385*, eadi3338. https://doi.org/10.1126/science.adi3338.

6. Chen, T., Nomura, K., Wang, X., Sohrabi, R., Xu, J., Yao, L., Paasch, B.C., Ma, L., Kremer, J., Cheng, Y., et al. (2020). A plant genetic network for preventing dysbiosis in the phyllosphere. Nature *580*, 653–657. https://doi.org/10.1038/s41586-020-2185-0.

7. Chaudhry, V., Runge, P., Sengupta, P., Doehlemann, G., Parker, J.E., and Kemen, E. (2021). Shaping the leaf microbiota: plant–microbe–microbe interactions. J Exp Bot *72*, 36–56. https://doi.org/10.1093/jxb/eraa417.

8. Schäfer, M., Pacheco, A.R., Künzler, R., Bortfeld-Miller, M., Field, C.M., Vayena, E., Hatzimanikatis, V., and Vorholt, J.A. (2023). Metabolic interaction models recapitulate leaf microbiota ecology. Science *381*, eadf5121. https://doi.org/10.1126/science.adf5121.

9. Banerjee, S., Schlaeppi, K., and van der Heijden, M.G.A. (2018). Keystone taxa as drivers of microbiome structure and functioning. Nat Rev Microbiol *16*, 567–576. https://doi.org/10.1038/s41579-018-0024-1.

10. Röttjers, L., and Faust, K. (2019). Can we predict keystones? Nat Rev Microbiol *17*, 193–193. https://doi.org/10.1038/s41579-018-0132-y.

11. Durán, P., Thiergart, T., Garrido-Oter, R., Agler, M., Kemen, E., Schulze-Lefert, P., and Hacquard, S. (2018). Microbial Interkingdom Interactions in Roots Promote Arabidopsis Survival. Cell *175*, 973-983.e14. https://doi.org/10.1016/j.cell.2018.10.020.

12. Lindsay, R.J., Pawlowska, B.J., and Gudelj, I. (2019). Privatization of public goods can cause population decline. Nat Ecol Evol *3*, 1206–1216. https://doi.org/10.1038/s41559-019-0944-9.

13. Thiergart, T., Durán, P., Ellis, T., Vannier, N., Garrido-Oter, R., Kemen, E., Roux, F., Alonso-Blanco, C., Ågren, J., Schulze-Lefert, P., et al. (2020). Root microbiota assembly and adaptive differentiation among European Arabidopsis populations. Nat Ecol Evol *4*, 122–131. https://doi.org/10.1038/s41559-019-1063-3.

14. Singh, B.K., Jiang, G., Wei, Z., Sáez-Sandino, T., Gao, M., Liu, H., and Xiong, C. (2025). Plant pathogens, microbiomes, and soil health. Trends in Microbiology *33*, 887–902. https://doi.org/10.1016/j.tim.2025.03.013.

15. Henry, L.P., Rat, A., Laderman, E., Lion, R., Mayjonade, B., Pathocom, T., Roux, F., Weigel, D., and Bergelson, J. (2025). Seasonality, land use, and diversity shape microbiome-pathogen interactions in wild populations of Arabidopsis thaliana. Preprint at bioRxiv, https://doi.org/10.1101/2025.06.29.662221 https://doi.org/10.1101/2025.06.29.662221.

16. Gao, M., Xiong, C., Gao, C., Tsui, C.K.M., Wang, M.-M., Zhou, X., Zhang, A.-M., and Cai, L. (2021). Disease-induced changes in plant microbiome assembly and functional adaptation. Microbiome *9*, 187. https://doi.org/10.1186/s40168-021-01138-2.

17. Kemen, E., Mahmoudi, M., Hu, Y., Almario, J., Stincone, P., Tenzer, L.-M., Chaudhry, V., and Nieselt, K. (2025). Machine Learning Reveals Biocontrol Agents Shaping Disease Protection in Natural Arabidopsis Populations and Synthetic Communities. Preprint at Research Square, https://doi.org/10.21203/rs.3.rs-6130404/v1 https://doi.org/10.21203/rs.3.rs-6130404/v1.

18. Taguas, I., Maclot, F., Montes, N., Pagán, I., Fraile, A., and García-Arenal, F. (2025). Infection Patterns of Albugo laibachii and Effect on Host Survival and Reproduction in a Wild Population of Arabidopsis thaliana. Plants *14*, 568. https://doi.org/10.3390/plants14040568.

19. Ploch, S., and Thines, M. (2011). Obligate biotrophic pathogens of the genus Albugo are widespread as asymptomatic endophytes in natural populations of Brassicaceae. Molecular Ecology *20*, 3692–3699. https://doi.org/10.1111/j.1365-294X.2011.05188.x.

20. Tronsmo, A.M., Munk, L., Djurle, A., and Collinge, D.B. (2020). The disease cycle and lifestyles. Plant Pathology and Plant Diseases *19*.

21. Agler, M.T., Ruhe, J., Kroll, S., Morhenn, C., Kim, S.-T., Weigel, D., and Kemen, E.M. (2016). Microbial Hub Taxa Link Host and Abiotic Factors to Plant Microbiome Variation. PLOS Biology *14*, e1002352. https://doi.org/10.1371/journal.pbio.1002352.

22. Gómez-Pérez, D., Schmid, M., Chaudhry, V., Hu, Y., Velic, A., Maček, B., Ruhe, J., Kemen, A., and Kemen, E. (2023). Proteins released into the plant apoplast by the obligate parasitic protist Albugo selectively repress phyllosphere-associated bacteria. New Phytologist *239*, 2320–2334. https://doi.org/10.1111/nph.18995.

23. Eitzen, K., Sengupta, P., Kroll, S., Kemen, E., and Doehlemann, G. (2021). A fungal member of the Arabidopsis thaliana phyllosphere antagonizes Albugo laibachii via a GH25 lysozyme. eLife *10*, e65306. https://doi.org/10.7554/eLife.65306.

24. Kemen, E., Gardiner, A., Schultz-Larsen, T., Kemen, A.C., Balmuth, A.L., Robert-Seilaniantz, A., Bailey, K., Holub, E., Studholme, D.J., MacLean, D., et al. (2011). Gene Gain and Loss during Evolution of Obligate Parasitism in the White Rust Pathogen of Arabidopsis thaliana. PLOS Biology *9*, e1001094. https://doi.org/10.1371/journal.pbio.1001094.

25. Lundberg, D.S., Lebeis, S.L., Paredes, S.H., Yourstone, S., Gehring, J., Malfatti, S., Tremblay, J., Engelbrektson, A., Kunin, V., Rio, T.G. del, et al. (2012). Defining the core *Arabidopsis thaliana* root microbiome. Nature *488*, 86–90. https://doi.org/10.1038/nature11237.

26. Watts, S.C., Ritchie, S.C., Inouye, M., and Holt, K.E. (2018). FastSpar: rapid and scalable correlation estimation for compositional data. Bioinformatics *35*, 1064. https://doi.org/10.1093/bioinformatics/bty734.

27. Hardoim, P.R., van Overbeek, L.S., Berg, G., Pirttilä, A.M., Compant, S., Campisano, A., Döring, M., and Sessitsch, A. (2015). The Hidden World within Plants: Ecological and Evolutionary Considerations for Defining Functioning of Microbial Endophytes. Microbiology and Molecular Biology Reviews *79*, 293–320. https://doi.org/10.1128/mmbr.00050-14.

28. Martín González, A.M., Dalsgaard, B., and Olesen, J.M. (2010). Centrality measures and the importance of generalist species in pollination networks. Ecological Complexity *7*, 36–43. https://doi.org/10.1016/j.ecocom.2009.03.008.

29. Banerjee, S., Walder, F., Büchi, L., Meyer, M., Held, A.Y., Gattinger, A., Keller, T., Charles, R., and van der Heijden, M.G.A. (2019). Agricultural intensification reduces microbial network complexity and the abundance of keystone taxa in roots. The ISME Journal *13*, 1722–1736. https://doi.org/10.1038/s41396-019-0383-2.

30. Hassani, M.A., Durán, P., and Hacquard, S. (2018). Microbial interactions within the plant holobiont. Microbiome *6*, 58. https://doi.org/10.1186/s40168-018-0445-0.

31. Chaudhry, V., Runge, P., Sengupta, P., Doehlemann, G., Parker, J.E., and Kemen, E. (2021). Shaping the leaf microbiota: plant-microbe-microbe interactions. J Exp Bot *72*, 36–56. https://doi.org/10.1093/jxb/eraa417.

32. Sohrabi, R., Paasch, B.C., Liber, J.A., and He, S.Y. (2023). Phyllosphere Microbiome. Annu Rev Plant Biol *74*, 539–568. https://doi.org/10.1146/annurev-arplant-102820-032704.

33. Jarrige, D., Haridas, S., Bleykasten-Grosshans, C., Joly, M., Nadalig, T., Sancelme, M., Vuilleumier, S., Grigoriev, I.V., Amato, P., and Bringel, F. (2022). High-quality genome of the basidiomycete yeast Dioszegia hungarica PDD-24b-2 isolated from cloud water. G3 Genes|Genomes|Genetics *12*, jkac282. https://doi.org/10.1093/g3journal/jkac282.

34. Enjo, F., Nosaka, K., Ogata, M., Iwashima, A., and Nishimura, H. (1997). Isolation and characterization of a thiamin transport gene, THI10, from Saccharomyces cerevisiae. J Biol Chem *272*, 19165–19170. https://doi.org/10.1074/jbc.272.31.19165.

35. Ahn, I.-P., Kim, S., and Lee, Y.-H. (2005). Vitamin B1 Functions as an Activator of Plant Disease Resistance. Plant Physiol *138*, 1505–1515. https://doi.org/10.1104/pp.104.058693.

36. Saharan, G.S., and Verma, P.R. (1992). White Rusts: A Review of Economically Important Species (International Development Research Centre).

37. Takashima, M., Manabe, R., and Ohkuma, M. (2019). Draft Genome Sequences of Basidiomycetous Epiphytic Phylloplane Yeast Type Strains Dioszegia crocea JCM 2961 and Dioszegia aurantiaca JCM 2956. Microbiol Resour Announc *8*, e01727-18. https://doi.org/10.1128/MRA.01727-18.

38. Connell, L.B., Redman, R., Rodriguez, R., Barrett, A., Iszard, M., and Fonseca, Á. (2010). Dioszegia antarctica sp. nov. and Dioszegia cryoxerica sp. nov., psychrophilic basidiomycetous yeasts from polar desert soils in Antarctica. Int J Syst Evol Microbiol *60*, 1466–1472. https://doi.org/10.1099/ijs.0.015412-0.

629 39. Wertheim, J.O., Murrell, B., Smith, M.D., Kosakovsky Pond, S.L., and Scheffler, K. (2015). RELAX:
630 Detecting Relaxed Selection in a Phylogenetic Framework. Molecular Biology and Evolution *32*,
631 820–832. https://doi.org/10.1093/molbev/msu400.

632 40. Takashima, M., and Nakase, T. (2011). Dioszegia Zsolt emend. Takashima, Deák & Nakase (2001).
633 In The Yeasts (Elsevier), pp. 1747–1757. https://doi.org/10.1016/B978-0-444-52149-1.00141-5.

634 41. Torres, D.E., Reckard, A.T., Klocko, A.D., and Seidl, M.F. (2023). Nuclear genome organization in
635 fungi: from gene folding to Rabl chromosomes. FEMS Microbiology Reviews *47*, fuad021.
636 https://doi.org/10.1093/femsre/fuad021.

637 42. Tuller, T., Carmi, A., Vestsigian, K., Navon, S., Dorfan, Y., Zaborske, J., Pan, T., Dahan, O., Furman,
638 I., and Pilpel, Y. (2010). An Evolutionarily Conserved Mechanism for Controlling the Efficiency of
639 Protein Translation. Cell *141*, 344–354. https://doi.org/10.1016/j.cell.2010.03.031.

640 43. Man, O., and Pilpel, Y. (2007). Differential translation efficiency of orthologous genes is involved
641 in phenotypic divergence of yeast species. Nat Genet *39*, 415–421.
642 https://doi.org/10.1038/ng1967.

643 44. Sonenberg, N., and Hinnebusch, A.G. (2009). Regulation of Translation Initiation in Eukaryotes:
644 Mechanisms and Biological Targets. Cell *136*, 731–745.
645 https://doi.org/10.1016/j.cell.2009.01.042.

646 45. Reis, M. dos, Savva, R., and Wernisch, L. (2004). Solving the riddle of codon usage preferences: a
647 test for translational selection. Nucleic Acids Res *32*, 5036–5044.
648 https://doi.org/10.1093/nar/gkh834.

649 46. Guerreiro, M.A., Yurkov, A., Nowrousian, M., Broders, K., and Stukenbrock, E. (2024). Genomic
650 and physiological signatures of adaptation in pathogenic fungi. Preprint at Research Square,
651 https://doi.org/10.21203/rs.3.rs-5041869/v1 https://doi.org/10.21203/rs.3.rs-5041869/v1.

652 47. dos Reis, M., Wernisch, L., and Savva, R. (2003). Unexpected correlations between gene
653 expression and codon usage bias from microarray data for the whole Escherichia coli K-12
654 genome. Nucleic Acids Res *31*, 6976–6985. https://doi.org/10.1093/nar/gkg897.

655 48. Gilchrist, C.L.M., and Chooi, Y.-H. (2021). clinker & clustermap.js: automatic generation of gene
656 cluster comparison figures. Bioinformatics *37*, 2473–2475.
657 https://doi.org/10.1093/bioinformatics/btab007.

658 49. Richards, T.A., and Talbot, N.J. (2013). Horizontal gene transfer in osmotrophs: playing with
659 public goods. Nat Rev Microbiol *11*, 720–727. https://doi.org/10.1038/nrmicro3108.

660 50. Lindsay, R.J., Kershaw, M.J., Pawlowska, B.J., Talbot, N.J., and Gudelj, I. (2016). Harbouring
661 public good mutants within a pathogen population can increase both fitness and virulence. eLife
662 *5*, e18678. https://doi.org/10.7554/eLife.18678.

663 51. Xia, C., Zhao, Y., Zhang, L., Li, X., Cheng, Y., Wang, D., Xu, C., Qi, M., Wang, J., Guo, X., et al.
664 (2023). Myxobacteria restrain Phytophthora invasion by scavenging thiamine in soybean
665 rhizosphere via outer membrane vesicle-secreted thiaminase I. Nat Commun *14*, 5646.
666 https://doi.org/10.1038/s41467-023-41247-0.

667 52. Backman, T., Latorre, S.M., Symeonidi, E., Muszyński, A., Bleak, E., Eads, L., Martinez-Koury, P.I.,
668 Som, S., Hawks, A., Gloss, A.D., et al. (2024). A phage tail–like bacteriocin suppresses

competitors in metapopulations of pathogenic bacteria. Science *384*, eado0713. https://doi.org/10.1126/science.ado0713.

53. Jaswal, K., Todd, O.A., Flores Audelo, R.C., Santus, W., Paul, S., Duffy, C.M., Eshoo, E.T., Singh, M., Miao, J., Underhill, D.M., et al. (2025). Commensal yeast promotes Salmonella Typhimurium virulence. Nature *645*, 1002–1010. https://doi.org/10.1038/s41586-025-09415-y.

54. Duan, S., Jin, Z., Zhang, L., and Declerck, S. (2025). Mechanisms of cooperation in the plants-arbuscular mycorrhizal fungi-bacteria continuum. The ISME Journal *19*, wraf023. https://doi.org/10.1093/ismejo/wraf023.

55. Morris, J.J., Lenski, R.E., and Zinser, E.R. (2012). The Black Queen Hypothesis: Evolution of Dependencies through Adaptive Gene Loss. mBio *3*, 10.1128/mbio.00036-12. https://doi.org/10.1128/mbio.00036-12.

56. Gregor, R., Vercelli, G.T., Szabo, R.E., Gralka, M., Reynolds, R.C., Qu, E.B., Levine, N.M., and Cordero, O.X. (2024). Vitamin auxotrophies shape microbial community assembly in the ocean. Preprint at bioRxiv, https://doi.org/10.1101/2023.10.16.562604 https://doi.org/10.1101/2023.10.16.562604.

57. Ryback, B., Bortfeld-Miller, M., and Vorholt, J.A. (2022). Metabolic adaptation to vitamin auxotrophy by leaf-associated bacteria. ISME J *16*, 2712–2724. https://doi.org/10.1038/s41396-022-01303-x.

58. Culp, E.J., and Goodman, A.L. (2023). Cross-feeding in the gut microbiome: Ecology and mechanisms. Cell Host & Microbe *31*, 485–499. https://doi.org/10.1016/j.chom.2023.03.016.

59. Sharma, V., Rodionov, D.A., Leyn, S.A., Tran, D., Iablokov, S.N., Ding, H., Peterson, D.A., Osterman, A.L., and Peterson, S.N. (2019). B-Vitamin Sharing Promotes Stability of Gut Microbial Communities. Front Microbiol *10*, 1485. https://doi.org/10.3389/fmicb.2019.01485.

60. Werner, G.D.A., and Kiers, E.T. (2015). Order of arrival structures arbuscular mycorrhizal colonization of plants. New Phytologist *205*, 1515–1524. https://doi.org/10.1111/nph.13092.

61. McIntosh, R.A., Plant Breeding Institute, The University of Sydney, Wellings, C.R., and Park, R.F. (1995). Wheat rusts: an atlas resistance genes (CSIRO).

Supplementary figures

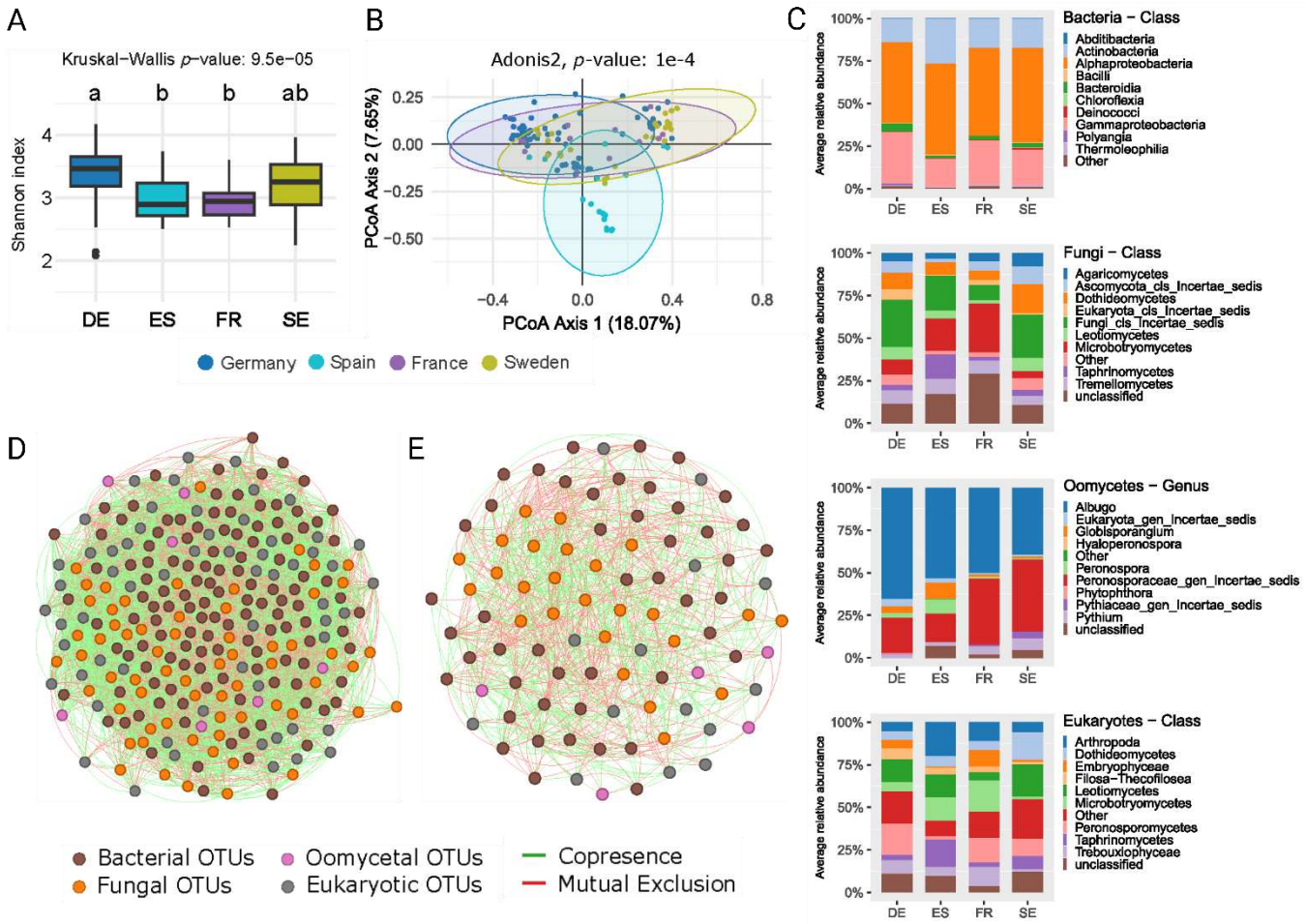


figure S1. Supporting evidence to the identification of *Albugo-Dioszegia* interactions. (A) α-diversity measures of whole leaf samples from different countries represented by Shannon index. Letters depict significant differences across countries (p<0.05, One-way ANOVA test). (B) Principle coordinate analysis (PCoA) based on Bray–Curtis distances between whole leaf samples from different countries. Each color represents all OTUs from the same country. (C) Relative abundance of the 10 most abundant taxa for each kingdom in whole leaf samples. Bacteria, fungi, and eukaryotes are represented at class level, oomycetes are represented at genus for better illustration since the total number of oomycete OTUs are lower compared to other kingdoms. (D) and (E) whole leaf network (D) and endophyte network (E), node and edge sizes unscaled. The edge color represents the type of interaction between two nodes as indicated.

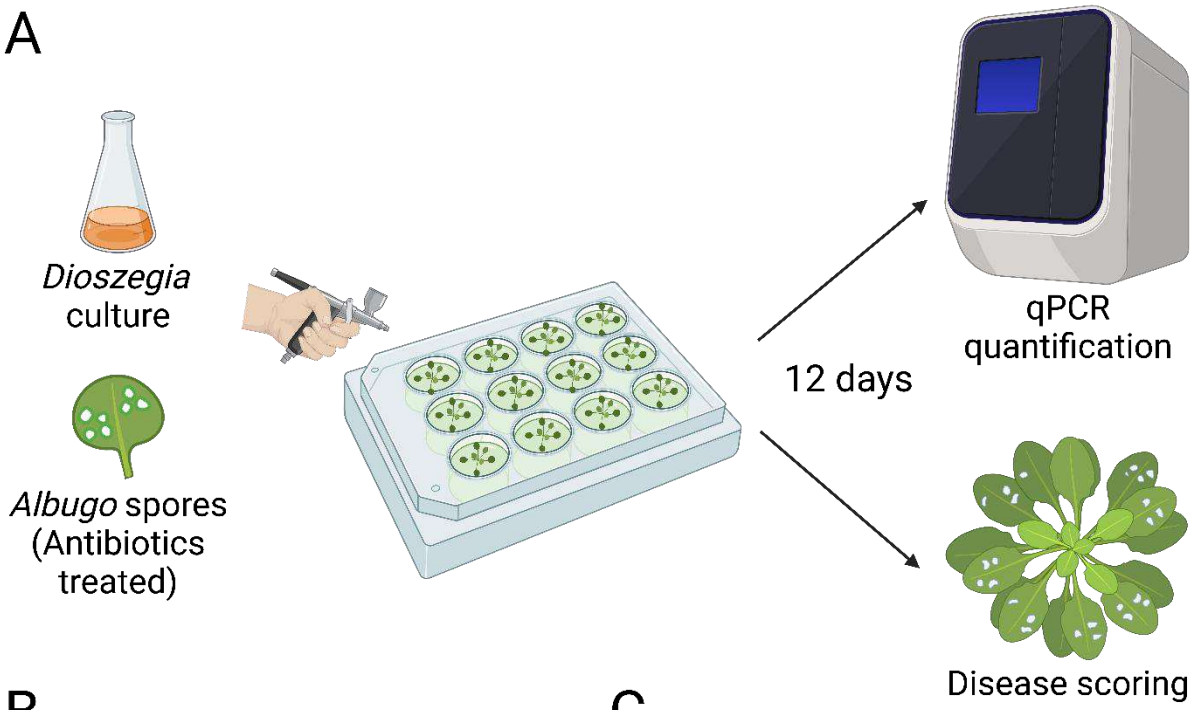


figure S2. The gnotobiotic system for testing the effect of microbes on the colonization of *A. laibachii*. (A) Workflow of the gnotobiotic co-cultivation of *Albugo* with different leaf associated microbes. The disease scoring is counting the average number of infected leaves for each plant. This figure was generated using BioRender (https://www.biorender.com/). (B) and (C) illustrates the symptom of filamentous fungi on sterile *A. thaliana*. Image (B) shows the 4 weeks old sterile *A. thaliana* seedlings 12 days after infection with *A. laibachii*. Image (C) shows 4 weeks old sterile *A. thaliana* seedlings 12 days after spraying with *A. laibachii* and *Fusarium* ERG.F51. Seedlings that did not grow well during the 4 week period were not included in the experiment. The two plates in each image represent technical replicates of each experiment.

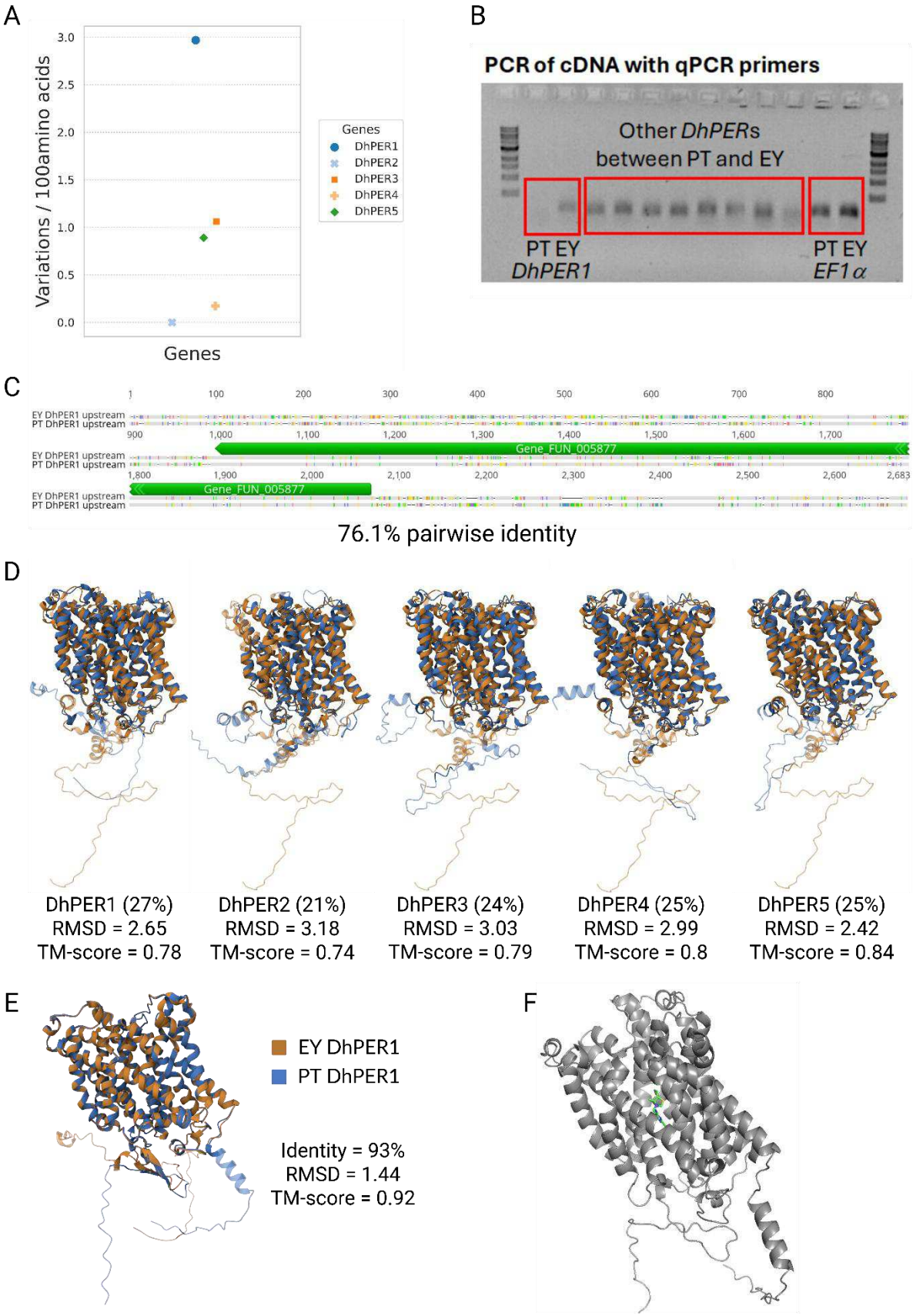


figure S3. Validation of *DhPER1* as the candidate gene responsible for the *Albugo* promotion. (A) Measurement of pairwise variations per 100 amino acids for predicted thiamine permeases of *Dioszegia* EY compared to PT. *DhPER1* showed the highest variation. (B) Agarose gel electrophoresis of RT-PCR for five *DhPERs in vitro* to assess the expression of the *DhPERs*. *DhPER1* showed expression in EY but not in PT, and all other *DhPERs* were

expressed in both strains. *EF1a* gene was used as a positive control of the PCR experiment. (C) Pairwise comparison of the 2kb upstream region of *Dioszegia* EY and PT *DhPER1* gene. The region was largely polymorphic, indicating a potential differential regulation of *DhPER1* expression in *Dioszegia* EY and PT. (D) Alignment of the Alphafold2-predicted structures of different *DhPERs* with that of *THI7* from *Saccharomyces cerevisiae* (UniProt A7A1C0_YEAS7) in ribbon representation. *DhPERs* are in orange and *THI7* is in blue color. (E) Alignment of the Alphafold2-predicted structures of *Dioszegia* EY and PT *DhPER1* in ribbon representation. (F) Molecular docking of the thiamine-HCl compound with *DhPER1* (grey color in ribbon representation) from *Dioszegia* PT using DiffDock (https://github.com/gcorso/DiffDock).

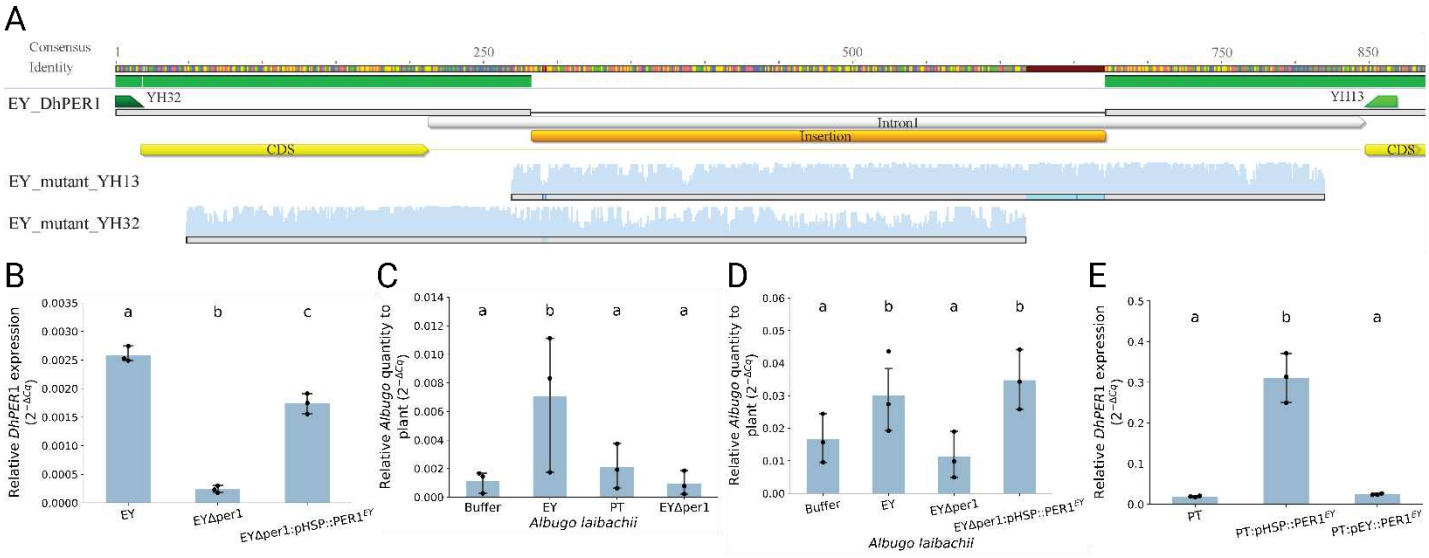


figure S4. Validation of *DhPER1*^{EY} knock out and complementation mutants. (A) Sanger sequencing validation of the 389 basepair insertion in EYΔper1 mutant. The EY_DhPER1 gene was used as reference and the primer used for sequencing was annotated. Forward and reverse reads were aligned to the reference sequences, with light blue peaks indicating the quality measure of each base. The insertion is highlighted in orange color. (B) Quantitative RT-qPCR validation of the *DhPER1* expression in *Dioszegia* EY mutants and complementation strains. The mutant was generated using the pHSP:CRISPR and pHSP:Hyg vectors, and the complementation strain was transformed using the pHSP:PER vector in the EYΔper1 mutant background. The *D. hungarica EF1a* gene was used as reference. The different letters represent significant difference from Tukey's HSD test results (p<0.01). (C) and (D) qPCR quantification of *A. laibachii* biomass normalized to *A. thaliana* biomass. Each data point represents DNA from 5-12 plants pooled together in each group, and three technical replicates were conducted from independent DNA extractions. Each datapoint in (C) was collected at a different time point (see supplementary methods for details). When these experiments were performed. we did not have the scoring data for this batch of samples since we had not finalized the scoring method. The data in (D) corresponds to the scoring data from Fig. 3B. Different letters represent significant differences in effect size between groups (Cohen's d > 0.8). (E) Quantitative RT-qPCR validation of the *DhPER1* expression in *Dioszegia* PT *DhPER1* complementation strains. The PT:pHSP::PER1^{EY} line was transformed using the pHSP:PER vector in the PT background, and the PT:pEY::PER1^{EY} line was transformed using the pEY:PER vector (see Materials and Methods).

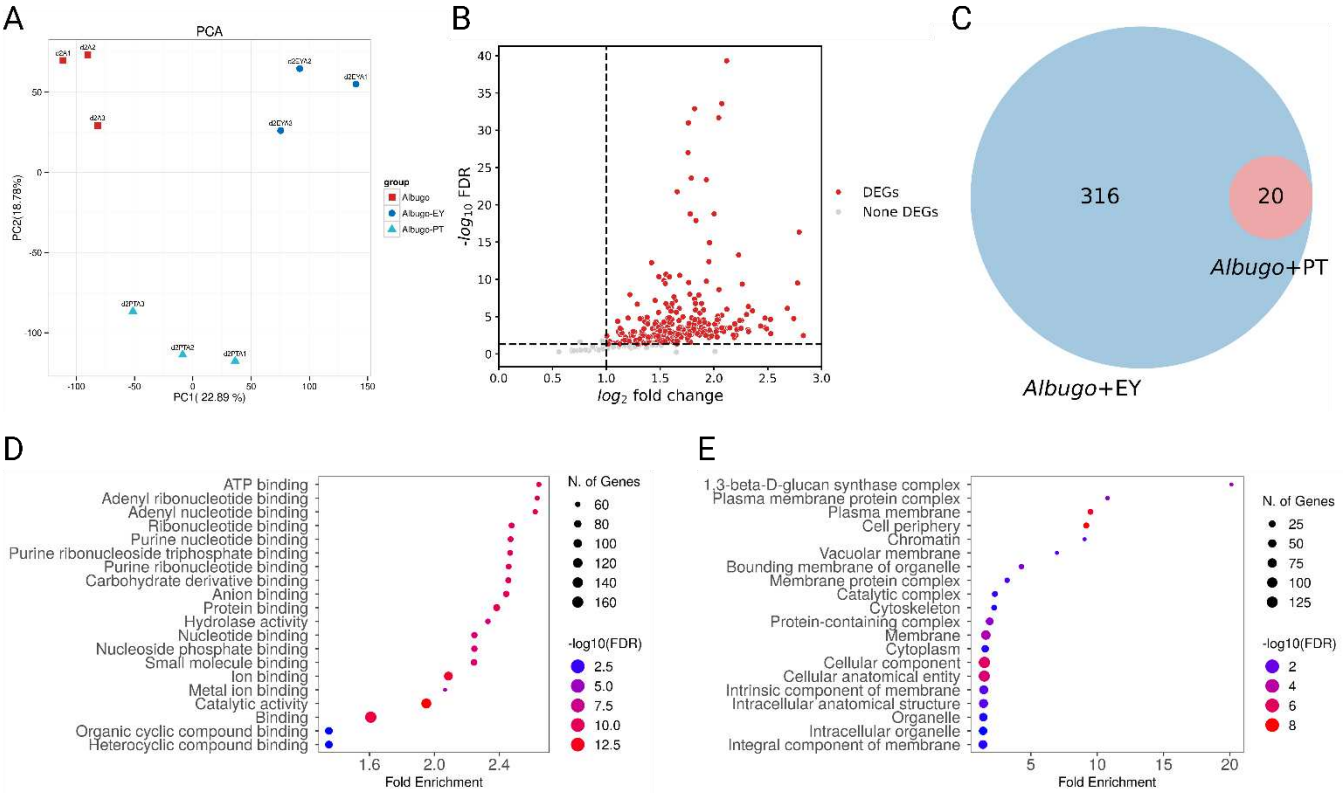


figure S5. RNA-seq analysis of 2 dai *A. laibachii* infected plants with *Dioszegia* EY and PT. (A) Principal component analysis(PCA) on FPKM of each sample from the RNA-seq experiment. Similarity among samples was displayed by reducing dimensionality into two or three principal components. (B) Volcano plot of all *A. laibachii* DEGs in the *Dioszegia* EY treated groups compared to buffer control. Red color represents all significant differential expression with $|\log_2 FC| > 1$ and FDR < 0.05 cut-off. (C) Venn diagram comparing the upregulated *A. laibachii* genes induced by *Dioszegia* EY and PT. (D) and (E) Dot plots showing the term enrichment analysis of GO: Cellular Component (D) and GO: Molecular Function (E) on all *A. laibachii* DEGs upregulated by *Dioszegia*. Top 20 enriched GO terms displayed, ranked by fold enrichment.

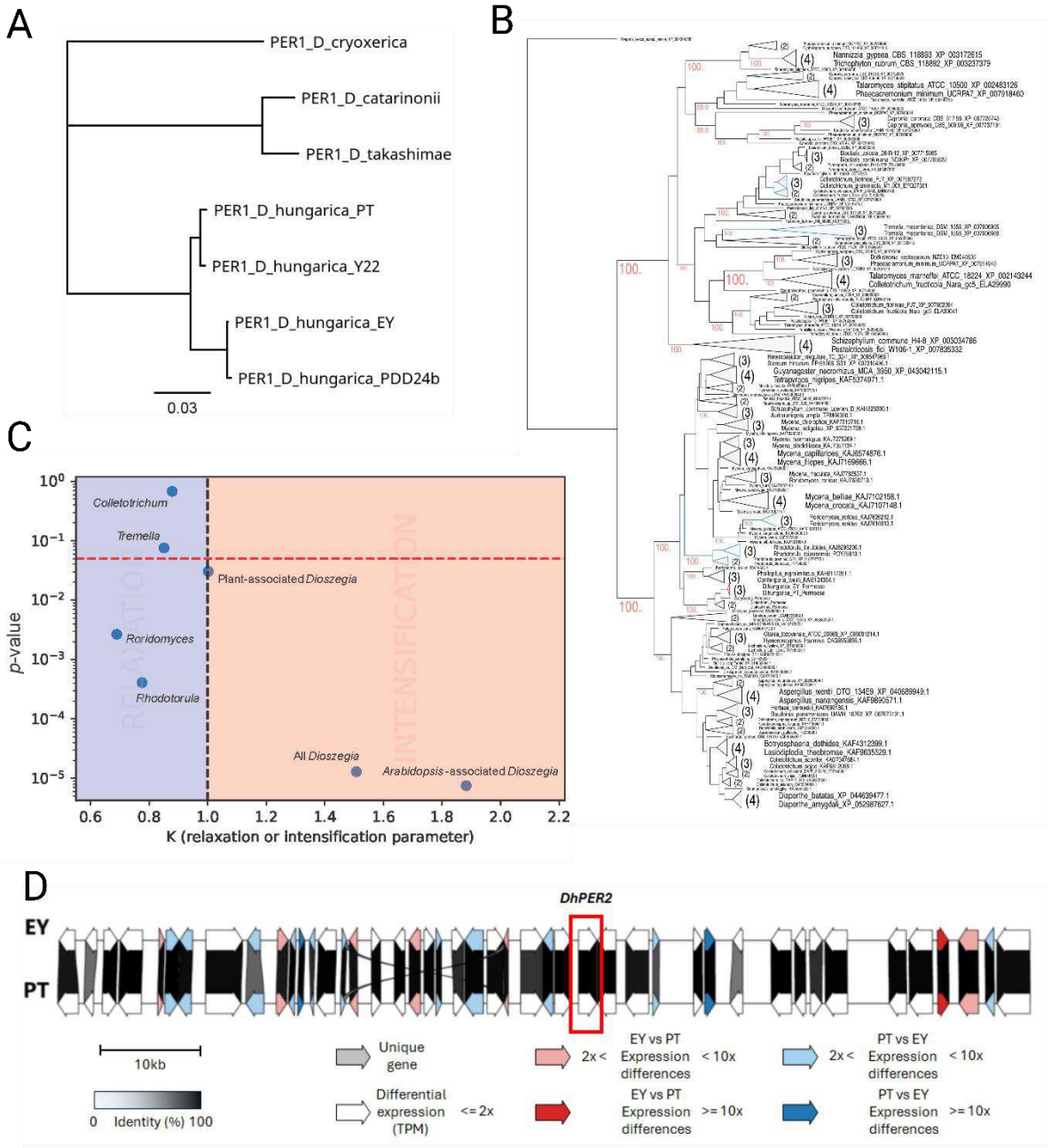


figure S6. Evolutionary analysis of *Dioszegia PER* genes. (A) Neighbor-joining tree of different *DhPER1* orthologous genes in different *Dioszegia* strains and species. The scale bar indicates 3% nucleotide sequence divergence. (B) Maximum likelihood phylogeny of *DhPER* hits from protein BLAST against a non-redundant database. The branches tested in (C) are highlighted in corresponding colors representing relaxed or intensified selection. (C) The Relax Selection test on different *DhPER* homologous genes belonging to different *Dioszegia* and other Basidiomycetes or Ascomycetes genera. (D) Global alignment of the 100kb *DhPER2* region using clinker[48]. Only orthologs with more than 35% protein identity (%) were annotated with linker. The color of each gene represents the transcriptional differences between each orthologs within this region.

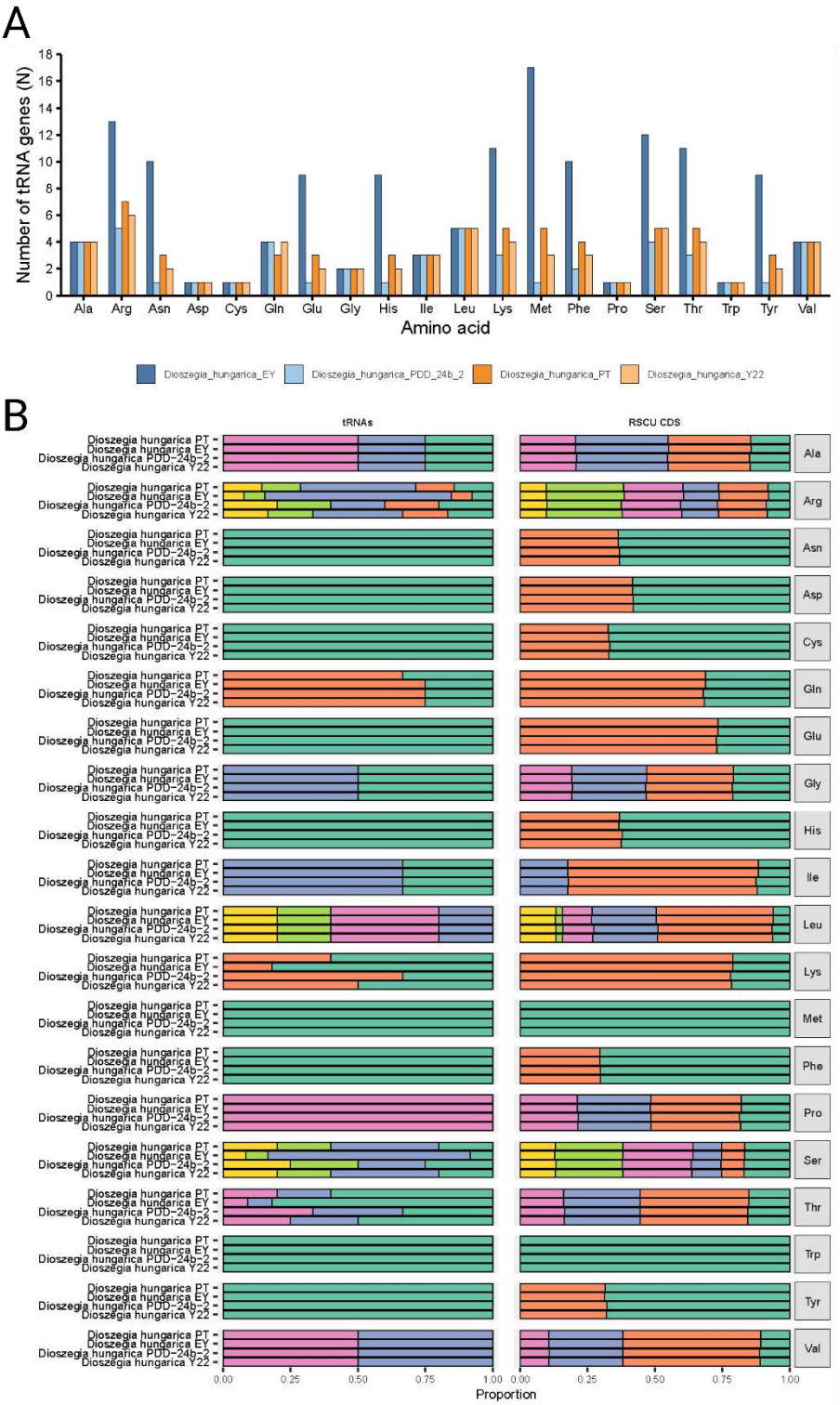


figure S7. Comparison of the tRNA content and relative synonymous codon usage (RSCU) for each amino acid among different *D. hungarica* strains. (A) Absolute number of tRNAs for each amino acid from genomes of four *D. hungarica* strains. (B) Proportion of synonymous codons for each amino acid across the coding sequence of four *D. hungarica* strains. The proportion of tRNA genes decoding the same codon and amino acid are given. For each dataset (tRNA or RSCU) and strain, each codon is color-coded for the same amino acid. However, the colours are independent across amino acids.

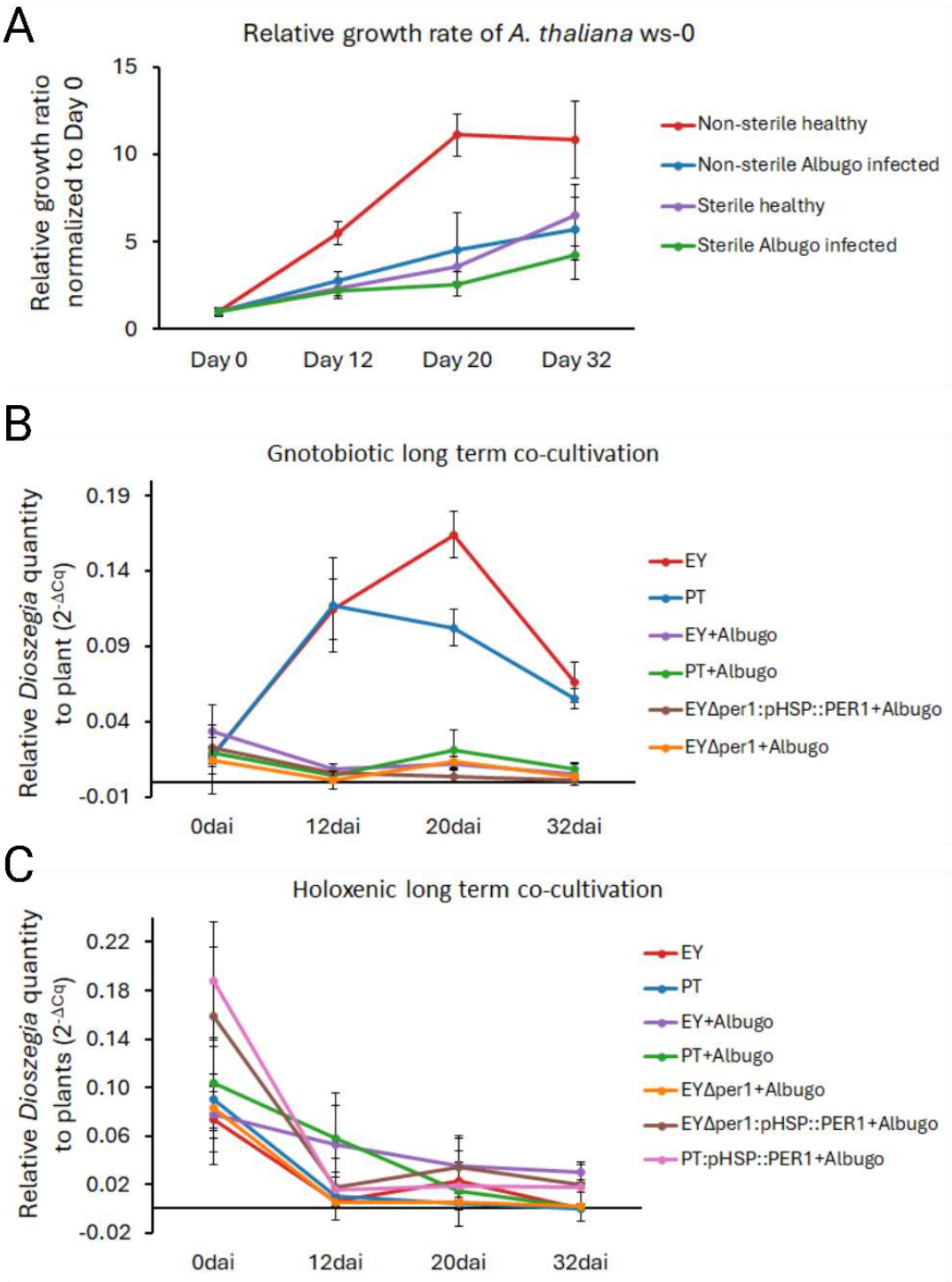


figure S8. Supplementary data to the long-term co-cultivation experiment. (A) Relative growth ratio calculated based on the fresh weight of *A. thaliana* ws-0 ecotype under sterile and non-sterile conditions. (B) and (C) The relative *Dioszegia* quantity measured by qPCR under gnotobiotic (B) and holoxenic conditions (C) in different treatment groups during the 32 day period. In both (B) and (C) the *DhEF1a* gene was used for qPCR and normalized to the *EF1a* gene from *A. thaliana.* In all panels, each time point shows the mean ± SE of 3 samples, and each sample contains three technical replicates.

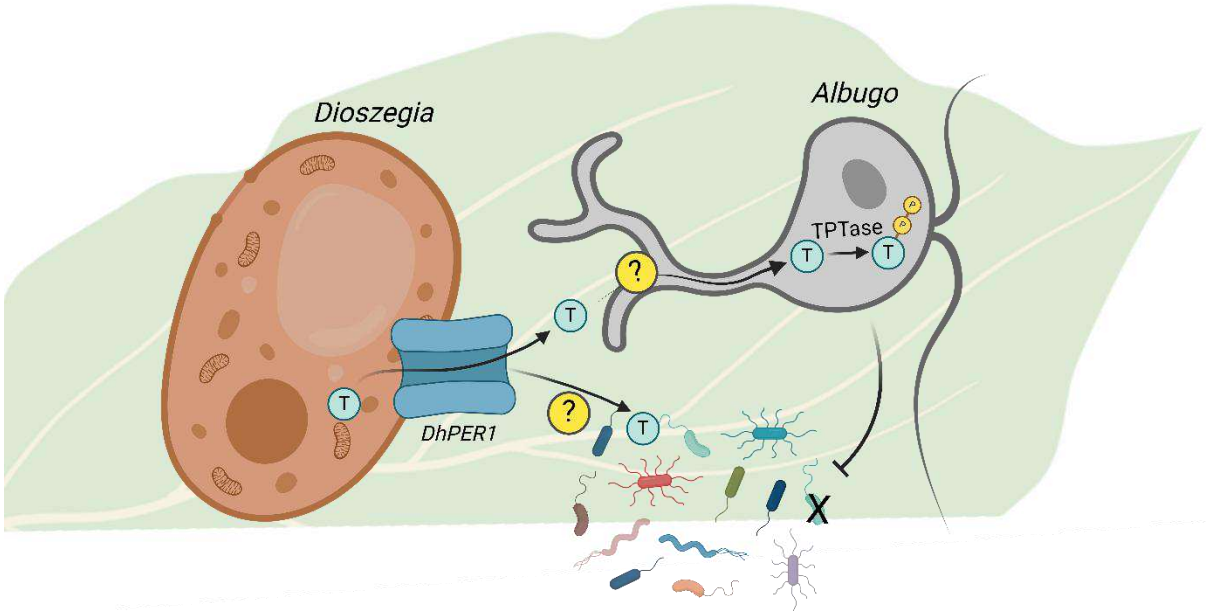


figure S9. The working model of *Dioszegia-Albugo* interactions in ecological context. The question mark indicates the thiamine transporter in the *Albugo* membrane. The figure was generated using BioRender.

table S1. List of interacting OTUs of A. laibachii OTU from oomycete amplicons. Yellow color highlighted the genera that we have tested in the gnotobiotic experiment.

table S2. Summary of all microbial strains used in this study.

table S3. Dioszegia genomes used and generated in this study. The basic stats of the genome is assess with stats.sh script from the BBmap package.

table S4. List of thiamine related genes in *Dioszegia* EY and PT and their percent ranks of tAI in each genomes.

table S5 : GPS coordinates and climatic variables of each site.

table S6. Oligo nucleotides used in this study. Different color fill represents primers used in different experiments.

Movies S1 & S2. *A. laibachii* zoospores interacting with *Dioszegia* EY cells. These two videos show a few hatched *A. laibachii* zoospores swimming and making contact with *Dioszegia* EY cells in a dense *Dioszegia* population. The *Dioszegia* EY cells were streaked from a fresh PDA plate, and the hatched *A. laibachii* zoospores (resuspended in water) was dropped on top of the *Dioszegia* cells. The time between frames is 0.167 s, and the video is sped up 10 times at 60 frames per second (FPS). Scale bar: 5 µm.

Movie S3. *A. laibachii* zoospore interacting with three *Dioszegia* EY cells. The video shows one hatched *A. laibachii* zoospore swimming and making contact with three *Dioszegia* EY cells. The *Dioszegia* EY cells were streaked from a fresh PDA plate, and the hatched *A. laibachii* zoospores (resuspended in water) was dropped on top of the *Dioszegia* cells. The videos were taken under the same condition as Movies S1&2. Scale bar: 5 µm.

Movie S4. *A. laibachii* zoospore interacting with one *Dioszegia* EY cell. The video shows a hatched *A. laibachii* zoospore swimming toward a *Dioszegia* EY cell. The videos were taken under the same condition as above movies. Scale bar: 5 µm.

Movies S5 & S6. Additional evidences of *A. laibachii* zoospores interacting with *Dioszegia* EY cells in various density. These two videos show in total of eight independent cases of *A. laibachii* zoospores interacting with *Dioszegia* EY cells. The videos were taken under the same condition as above movies. Scale bar: 5 µm.

Supplementary Files

This is a list of supplementary files associated with this preprint. Click to download.

- fig.S8.pdf
- MovieS1compressed.mp4
- MovieS4.mp4
- Supplementarytables.zip
- MovieS3compressed.mp4
- fig.S5.pdf
- MaterialsandMethods.pdf
- fig.S1.pdf
- fig.S7.pdf
- fig.S4.pdf
- MovieS6compressed.mp4
- MovieS5compressed.mp4
- fig.S3.pdf
- fig.S9.pdf
- fig.S6.pdf
- MovieS2compressed.mp4
- fig.S2.pdf